Journal of South American Earth Sciences 32 (2011) 438–459

Contents lists available at ScienceDirect

Journal of South American Earth Sciences

journal homepage: www.elsevier.com/locate/jsames

The age and tectonic setting of the Puncoviscana Formation in northwestern Argentina: An accretionary complex related to Early Cambrian closure of the Puncoviscana Ocean and accretion of the Arequipa-Antofalla block

Mónica P. Escayola [a,*], Cees R. van Staal [b], William J. Davis [c]

[a] CONICET- IDEAN, Instituto de Estudios Andinos, Laboratorio de Tectónica Andina, Universidad de Buenos Aires, Pabellón II, Nuñez, Buenos Aires, C1428EHA, Argentina
[b] Geological Survey of Canada. 625 Robson Street, Vancouver, V6B 5J3 BC, Canada
[c] Geological Survey of Canada. 601 Booth St. Ottawa K1S 4H7, ON, Canada

ARTICLE INFO

Article history:
Received 25 February 2011
Accepted 26 April 2011

Keywords:
Tilcarian–Pampean orogeny
Puncoviscana Ocean
Arequipa Antofalla

ABSTRACT

TIMS and SHRIMP U–Pb zircon geochronology of selected parts of the Puncoviscana Formation suggest its deposition took place mainly during the Early Cambrian, coeval with 540–535 Ma calc-alkaline Pampean arc volcanism mainly preserved as tuff beds in the oldest identified parts of this unit. Syn- to post-tectonic plutons constrains the Tilcarian–Pampean orogeny to have occurred between ca. 530 Ma and deposition of the unconformably overlying Middle-Upper Cambrian Meson Group. Deposition of the Puncoviscana Formation continued after the onset of the Tilcarian–Pampean orogeny. We propose that the Puncoviscana Formation rocks older than 530 Ma were deposited in the arc-trench gap of the west-facing Pampean arc and/or the associated trench, whereas the rocks younger than 530 Ma were deposited in a syn-collision foreland basin. The Puncoviscana Formation rocks were progressively assembled into a west-younging accretionary complex, consistent with the style of deformation and low-grade metamorphism. The age of the syn-collision plutons (≤530 Ma) suggest the foredeep deposits record the transition from trench to foreland basin, due to arrival of the Arequipa-Antofalla block at the west-facing trench at ca. 530 Ma. Our geochronological and Pb-isotope investigations suggest that the Arequipa-Antofalla terrane was a coherent, ribbon-shaped crustal block that also included the western part of the Pampia terrane. A compilation of existing U–Pb zircon studies suggests that the Pampean arc extended along the length of the proto-Andean margin of West Gondwana, represented by the previously amalgamated Amazonia and Rio de La Plata cratons, and probably was initiated during the late Ediacaran after 600 Ma.

Following earlier workers, we reaffirm that the Arequipa-Antofalla block was originally separating Laurentia and Amazonia in Rodinia. It probably rifted from Laurentia during the Ediacaran between 600 and 570 Ma, following an earlier departure of Amazonia (~650 Ma?). The separation of Arequipa-Antofalla from Amazonia and Laurentia opened the Puncoviscana and Iapetus oceans respectively.

1. Introduction

The Ediacaran to Early Cambrian tectonic history of the Central Andean basement is critical to fully comprehend the tectonic processes involved in the complex assembly of Western Gondwana (e.g. Cordani et al., 2009) and opening of the Iapetus Ocean. Based on several lines of evidence the Amazonian craton is generally considered the conjugate margin to the Appalachian margin of Laurentia in Rodinia (e.g. Hoffman, 1991; Dalziel, 1997; Tohver et al., 2002, 2004), although there are also alternative models (e.g. Evans, 2009). If Amazonia was indeed the conjugate margin it raises major tectonic questions. Particularly problematic is why ocean opening appears to have been accompanied by Ediacaran–Early Cambrian subduction and arc magmatism along large tracts of its assumed conjugate margin in South America (e.g. Escayola et al., 2007; Chew et al., 2007, 2008; Cardona et al., 2009) and replaced by the younger Famatinian arc system during the Ordovician (Rapela et al., 1998; Ramos, 2008). Widespread Early Paleozoic subduction along the proto-Andean margin indicates that opening of Iapetus was unlike the Atlantic Ocean with which it is commonly compared (Dalziel, 1997), but instead in some way related to the tectonic processes involved in the assembly of West Gondwana (Van Staal et al., 1998).

* Corresponding author. Tel.: +54 11 1558951729.
E-mail address: mescayola@gl.fcen.uba.ar (M.P. Escayola).

0895-9811/$ – see front matter © 2011 Elsevier Ltd. All rights reserved.
doi:10.1016/j.jsames.2011.04.013

An extensive reconnaissance study of the Neoproterozoic to Early Paleozoic rocks in northwestern Argentina (Fig. 1) led to selection of three key areas for a multidisciplinary study, mainly using U–Pb SHRIMP zircon provenance studies of sedimentary rocks, U–Pb geochronology (SHRIMP and TIMS) and Pb–Pb isotopic analyses of igneous rocks and assessment of the structural and metamorphic history. The Santa Victoria Oeste area, located immediately south of the Argentine–Bolivian border and the Quebrada de Huamahuaca were selected for study of the Puncoviscana Formation and associated igneous rocks (e.g. Cañani pluton). In addition, we investigated orthogneiss in the southern Domain of the Antofalla basement, west of the Antofalla Salt Flat.

2. Geological setting

2.1. Puncoviscana Formation

The Puncoviscana Formation of northern Argentina (Fig. 1) predominantly comprises a relatively thick sequence of alternating green sandstones, commonly graded, siltstones and mudstones of low- to very low metamorphic grade (e.g. Do Campo and Nieto, 2003). The finer grained lithologies (siltstones or mudstones) locally are red and interlayering of red and green sedimentary rocks is a distinct feature of this formation in several places (e.g. Quebrada de Huamahuaca) (Figs. 1, 2A). The outcrop pattern of the Puncoviscana Formation defines a series of narrow, north-south trending belts in the Puna and Eastern Cordillera (northwestern Argentina and southernmost Bolivia), which extend for more than 800 km parallel to the regional north-south strike over a width of circa 200 km (Figs. 1, 3). Higher grade metamorphic equivalents occur to the south of the town of Tucuman (Aceñolaza and Miller, 1982; Willner et al., 1987).

The thick sequence of green sandstone, siltstone and mudstone represents a distinct lithofacies in northern Argentina (e.g. Jezek et al., 1985) and all sedimentary rocks with these characteristics traditionally have been included in this unit, although it also include minor bodies of limestone and conglomerate. However, as will shown below, not all rocks previously included in the Puncoviscana Formation have the same age and may not have been deposited in the same basin or setting. For example, locally rocks as young as Ordovician have been included in the past in this unit by some workers (see Hausser et al., 2011), which cannot be correlated with the lower Cambrian rocks in the type locality (see below). Hence, in the absence of an adequate encompassing stratigraphic terminology, we collectively refer to these belts as the Puncoviscana tract and tried to exclude rocks that were not subjected to the typical style of tectonism of this unit as much as possible.

The silicilastic rocks mainly represent a sequence of turbidites (e.g. Jezek et al., 1985) and are generally inferred to be Ediacaran to Early Cambrian in age on basis of *Oldhamia*, and their position immediately below the unconformably overlying Middle to Upper Cambrian Meson Group (Aceñolaza et al., 1988; Adams et al., 2010). A remaining point of contention is whether the rocks are predominantly Neoproterozoic (Omarini et al., 1999) or Lower Cambrian (Durand and Aceñolaza, 1990). The Puncoviscana tract and associated pre-Middle Cambrian intrusives (see below) were involved in the Tilcarian–Pampean orogenic cycle, which had largely finished before deposition of the Middle to Upper Cambrian Meson Group.

Geochemistry (Zimmermann, 2005) of the Puncoviscana tract sandstones, suggest that they are volcanogenic with arc-like compositions (Fig. 4). This aspect will be discussed further below, but has not been appreciated previously in analyses mainly relying on classic petrological tools designed for unmetamorphosed sediments (e.g. Jezek et al., 1985; Jezek and Miller, 1987). However, pervasive low-grade metamorphism, evidenced by the formation of cleavage seams rich in chlorite and phengite (e.g. Do Campo and Nieto, 2003) suggest that solution transfer was an important deformation mechanism (see below). This process may have destroyed most of the original sedimentary constituents other than quartz and some albitised plagioclase clasts, which in turn may have seriously skewed analysis of the sedimentary petrology based on total feldspar content, unstable volcanic fragments and known mobile elements such as potassium and sodium (cf. Jezek et al., 1985; Jezek and Miller, 1987).

The Santa Victoria Oeste area is the type locality of the Punconviscana Formation (Fig. 1, localities 1 and 2). This unit was formally introduced here and mapped in detail by Turner (1960, 1964), who considered these rocks to be mainly Precambrian in age. In the village of Puncoviscana (Fig. 1, locality 1), the green wackes and mudstones are interlayered with thin pinkish or yellowish white felsic tuff beds (Fig. 2B) still containing relict, partially broken quartz phenocrysts and thin plagioclase-phyric basalt to andesite layers (50–100 cm). The volcanic origin of the latter could not be confirmed conclusively. In part they could also be narrow high-level sills. Regardles, the mafic igneous rocks were deformed and metamorphosed with the surrounding rocks and hence form an integral part of this formation in this locality. The felsic and mafic volcanic rocks have calc-alkaline compositions typical of an arc setting (see Section 6).

2.2. Deformation and metamorphism of the Puncoviscana Formation

The dominant structure in the Puncoviscana tract are tight, upright to inclined, commonly chevron-style folds (e.g. Willner et al., 1987; Piñan-Llamas and Simpson, 2006) with angular to rounded hinges and straight limbs (Fig. 2A, D). The folds are commonly accompanied by a slaty or domainal axial planar cleavage defined by white mica, optically identified as phengite (i.e. nearly uniaxial), and green chlorite. In the coarse wacke beds, the cleavage anastomoses around aligned quartz and plagioclase clasts. The clasts are commonly elongated as a result of truncation and dissolution along the cleavage planes and generally have mica (phengite) beards in the apexes where the cleavage planes converge. The mica beards and long axes of the quartz and albite clasts define a lineation. The clasts generally show little internal strain or evidence of recrystallization, suggesting that solution transfer was one of the principal deformation mechanisms. Fibrous extensional quartz veins with the fibres parallel to the foliation and the mica beard lineation also attest to the significance of fluids accommodating the deformation of these rocks (e.g. Van Staal et al., 2001 and references therein).

In several places, the deformation is demonstrably more complex and polyphase. Locally an older cleavage is folded by strongly inclined to recumbent tight to isoclinal folds (Figs. 2C, 5A), which are locally accompanied by a crenulation cleavage. These folds are locally associated with narrow or discrete bedding-parallel faults, which locally ramp-up through the earlier structures (Fig. 2C, D). Shear-sense indicators such as drag displayed by the pre-existing cleavage and offset of markers, show these faults to be mainly thrusts or reverse faults. We refer to the older folds and cleavages as the early structures and all the overprinting younger structures as the late structures. However, overprinting relationships suggest that the late structures probably include more than one generation of structures conform the observations of earlier workers (Willner et al., 1987).

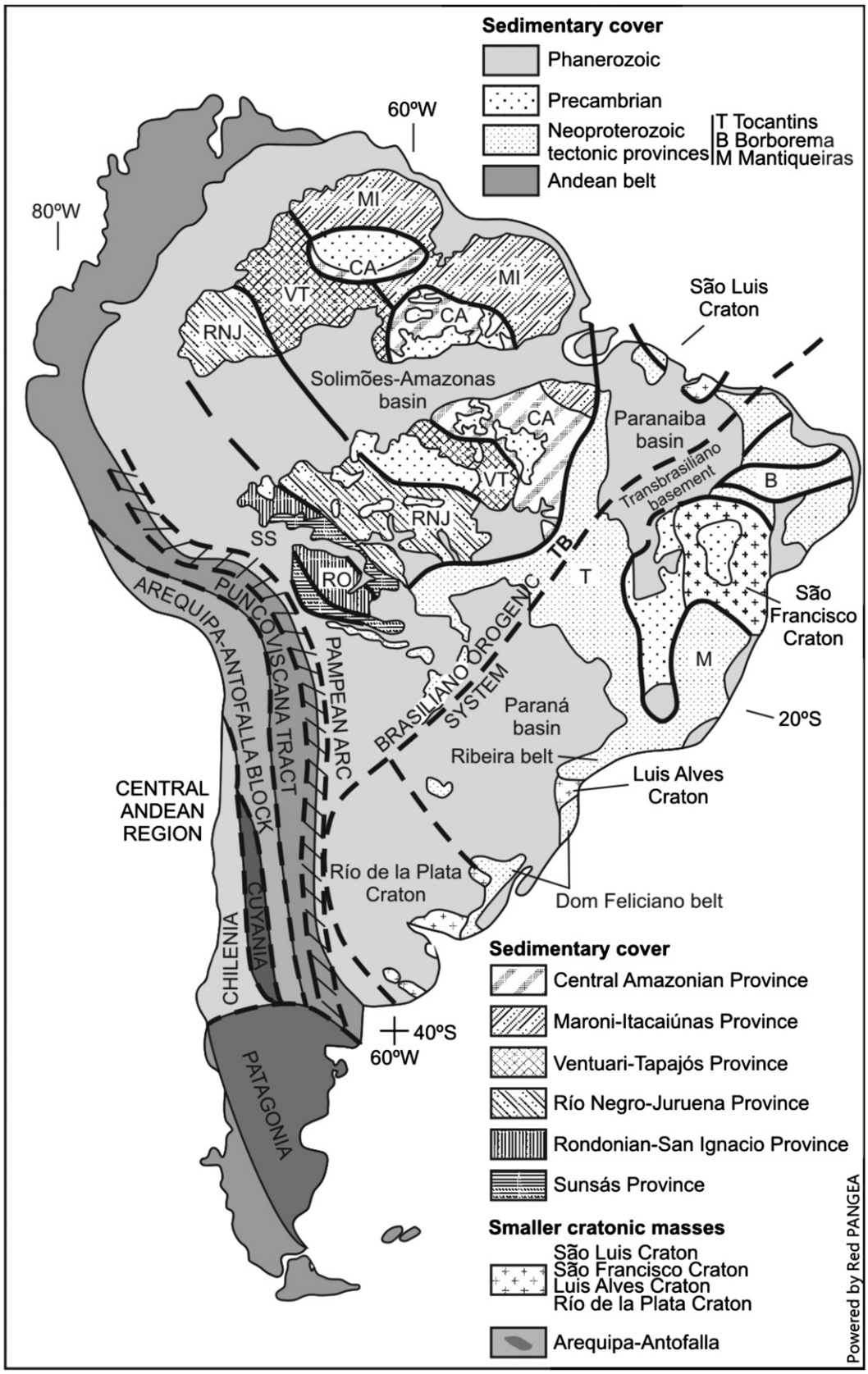

Fig. 1. Map of South America with the major tectonic provinces, modified from Chew et al. (2008) and Collo et al. (2009). Map show the approximate location of the Pampean arc and Arequipa-Antofalla block between 550 and 520 Ma, which are pertinent to the Pampean tectonic evolution of this part of South America. We extended the Pampean arc north up along the proto-Andean margin of West Gondwana, based on the interpretations of Chew et al. (2008). We also included the western part of the Pampia terrane of Ramos et al. (2010) with the Arequipa-Antofalla block. Note our interpretations differ from Ramos (2008) in that we keep the Arequipa and Antofalla terranes as one coherent ribbon-shaped block, instead of separating them in Late Neoproterozoic times, which only allows restricted opening of the Puncoviscana Ocean. The amalgamation of Amazonia and the Rio de La Plata cratons took place before 600 Ma (see Fig. 8) as a result of the closure of the Neoproterozoic Goiás Ocean.

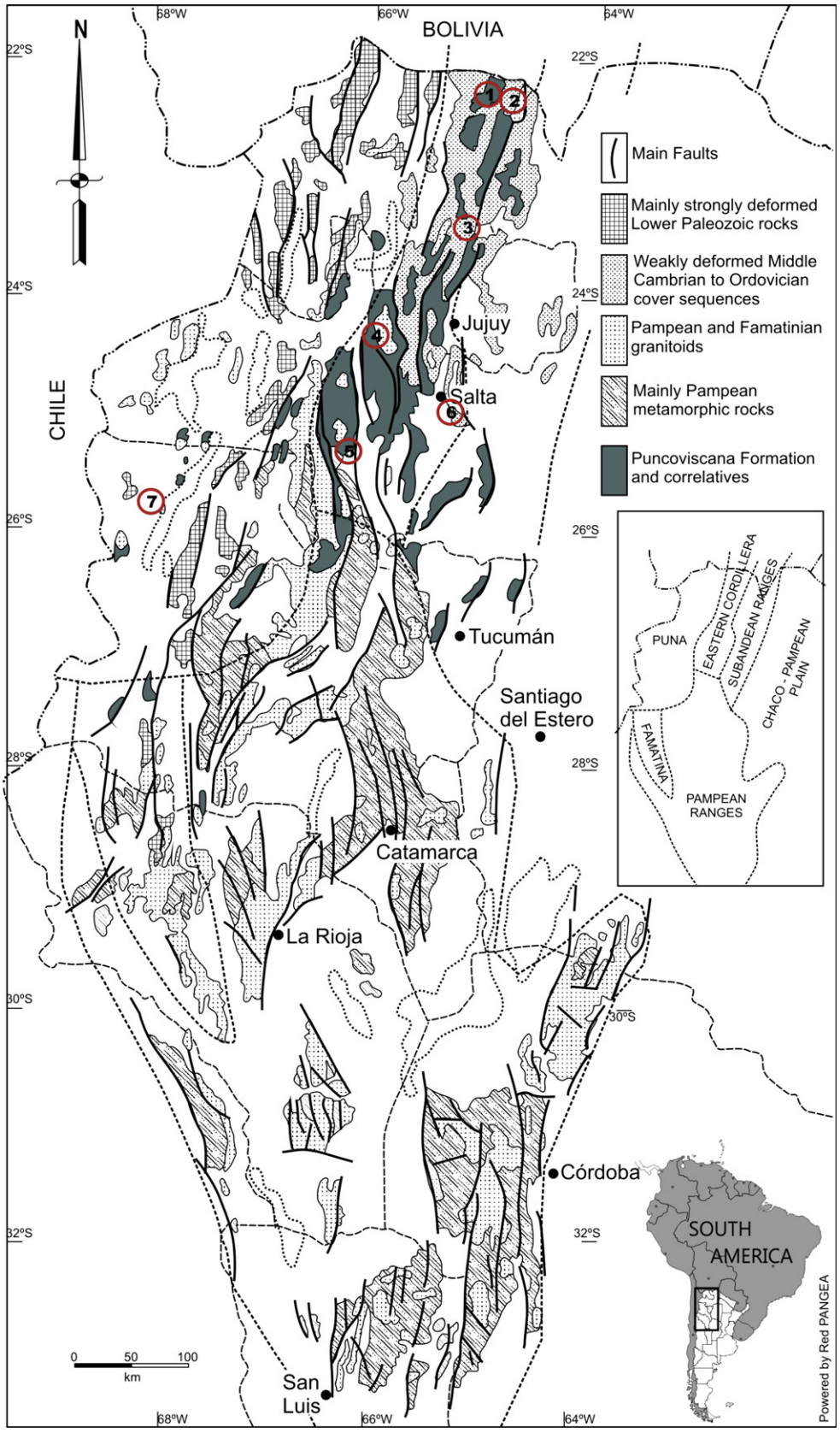

Fig. 2. Geological map with the distribution of the Lower Paleozoic and older units in northern and central Argentina, modified from Hongn et al. (2010). The distribution of the Puncoviscana formation outlines the Puncoviscana tract. The locations discussed in text are indicated by numerals: 1, Puncoviscana village locality; 2, Cañani pluton in Cañani Brook; 3, Quebrada de Huamahuaca; 4, Tastil granodiorite; 5, Corralito; 6, Las Tienditas; 7, Cerro Negro, Antofalla.

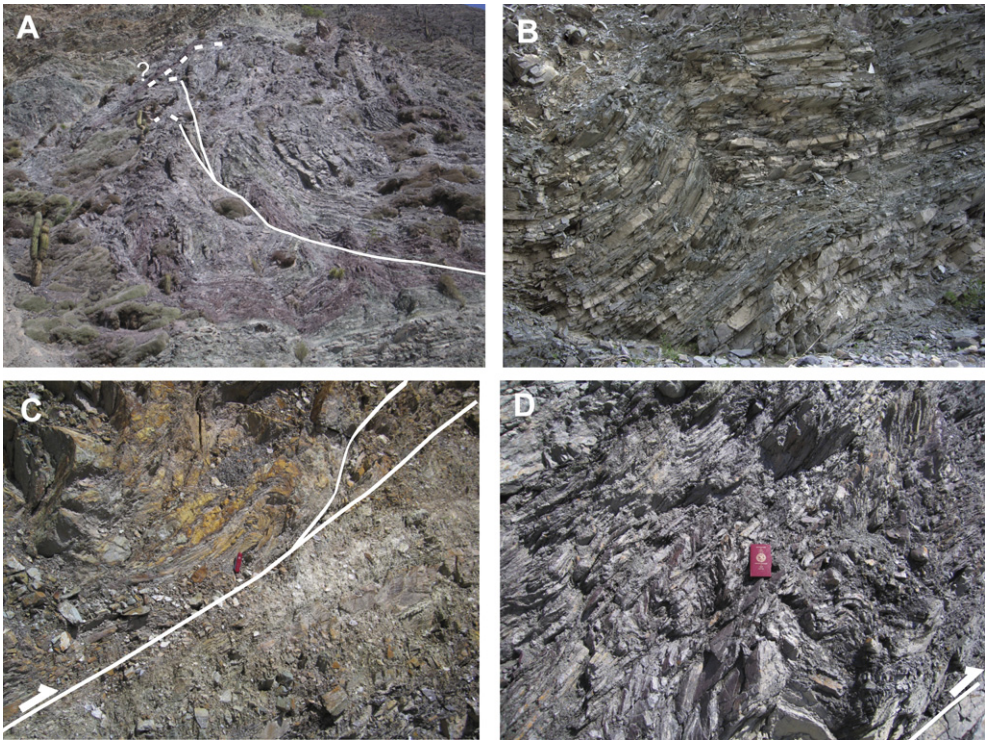

Fig. 3. (A) Interlayered green and red wackes and shales of the Puncoviscana Formation in a vertical cliff near Punmamarca (cactus at left is 2–3 m high), The rocks were deformed into tight chevron folds, which are cut by discrete thrusts that ramp-up towards the left and than appear to be folded by open folds near the top of the cliff or are cut-off by a younger thrust. The age of the thrusting is unknown, but if the apparent folding is correct it may be older than Andean. B. Interlayering of pinkish white felsic tuff beds with the Puncoviscana Formation near the village of Puncoviscana. The vertical width of the photo is approximately 3.5 m. (C) Northerly overturned, early recumbent fold in the hangingwall of a small thrust outlined by a brecciated zone and strongly foliated green wacke and siltstone near the village of Puncoviscana. The thrust has splays that ramp-up to the north. The Puncoviscana Formation here contains numerous bedding-parallel faults associated with the early chevron folds (D). Regionally these structures have been refolded by young north-south trending upright, open folds that also deform the unconformably overlying Meson and Santa Victoria groups (Turner, 1964). Knife for scale. (D) Inclined, northerly overturned early chevron folds in the immediate hangingwall of a southeast-dipping thrust plane located in strongly foliated shale bed visible in the right-lower corner. These structures occur close to locality (C). Fieldbook for scale. (For interpretation of the references to colour in this figure legend, the reader is referred to the web version of this article.)

The early folds are truncated by the Meson Group unconformity, which combined with the predominantly Early Cambrian age of most of the Puncoviscana tract rocks (see below) shows that these structures formed during the Early Cambrian Tilcarian-Pampian orogenic cycle (Aceñolaza and Toselli, 1976). Early Cambrian deformation is confirmed by relationships of the structures to Early Cambrian intrusions such as the Cañani and Tastil plutons discussed below. The age of the late structures is less well constrained. At least in part (e.g. recumbent folds and associated thrusts), they probably also formed during the Tilcarian, because these structures were not observed in the overlying Meson and Santa Victoria groups. These generally show much less intense and complex deformation and are typically folded into open north-south trending structures. Some of the larger structures are as young as Andean, which commonly have an easterly vergence in this area (Kley, 1996). At present it is difficult to separate and group the various structures on a regional scale. Furthermore, the lack of internal marker horizons complicates analysis of the overall macroscopic structure of the Puncoviscana tract and hence, assess the impact of the younger strain on the older, early structures.

The detailed mapping by Turner (1964) in the type locality suggests its structure was complex with the Puncovicana Formation typically exposed in the core of large fault-bounded antiforms. Some of these antiforms are partially reoriented and/or obliquely overprinted by younger structures, which also fold the unconformably overlying Meson and Santa Victoria groups.

The Puncoviscana Formation rocks investigated by us generally are penetratively metamorphosed to very low-grade conditions, defined mainly by chlorite, albite and phengite. The widespread presence of phengite in the Puncoviscana Formation was confirmed by Do Campo and Nieto (2003), whose chemical analyses of phengite suggest relatively high-pressure conditions (5–7 kbar). Prehnite and epidote are either very rare or absent in the green wackes and interlayered metabasalt, but fine-grained, bluish-green pumpellyite is locally possibly present, suggesting sub-greenschist facies metamorphic conditions ($\leq$350 °C) with burial depths sufficiently high to stabilize phengite. Such conditions support the relatively low temperature-high-pressure conditions (high-anchizonal to epizonal grade) determined by Do Campo and Nieto (2003). The latter authors locally also identified sporadic biotite, suggesting metamorphic conditions vary regionally across the Puncoviscana tract and range into the lower greenschist facies. Such metamorphic conditions are consistent with the microstructural evidence that recrystallization of quartz and albite was insignificant or absent and solution transfer the dominant deformation mechanism. The dominance of solution transfer and the metamorphic assemblages suggest temperatures lower than 350 °C for the rocks studied by us, which lack biotite (Van Staal et al., 2001, 2008) and possibly slightly higher (350–400 °C) where biotite is present (Do Campo and Nieto, 2003).

2.3. Early Cambrian Tilcarian-related intrusions

2.3.1. Cañani pluton

The Cañani pluton lies east of Santa Victoria Oeste (Fig. 1 – locality 2) and intruded the Puncoviscana Formation. The intrusion comprises two facies: hornblende-biotite granodiorite to quartz diorite and biotite-hornblende diorite. Small, hornblende-rich

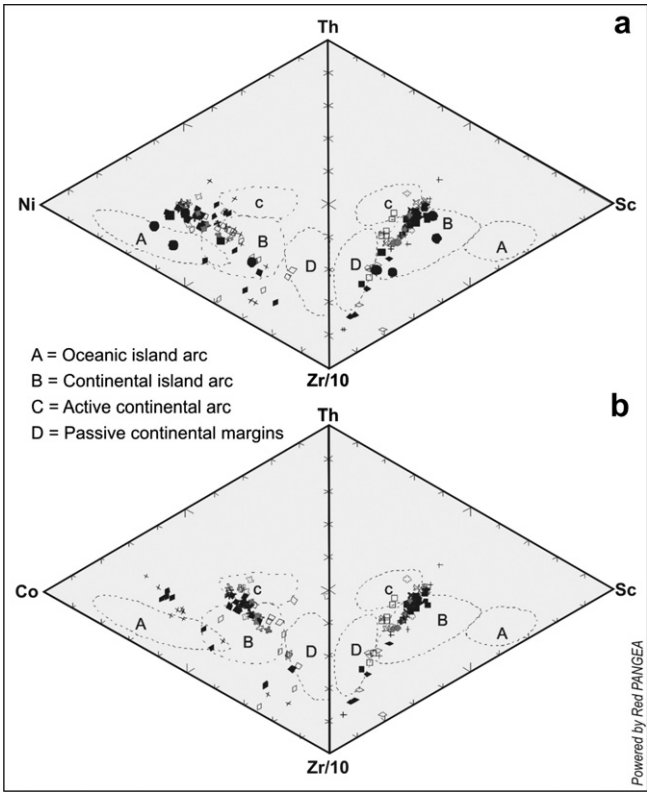

Fig. 4. Geochemical data of the Puncoviscana Formation from Zimmermann (2005) and presented in this paper plotted in the Th–Sc–Zr/10 and Th–Co–Zr/10 after Bhathia and Crook (1986). Most of the samples fall in the Continental Arc–Continental Island arc field indicating a provenance related to a magmatic source.

melanocratic diorite enclaves (Fig. 5B) are common in the more leucocratic phases. The pluton is situated in the core of a north-south trending antiform (Fig. 1), which is truncated by a relatively late east-verging reverse fault along its eastern limb (Turner, 1964). Both the antiform and reverse fault are late structures because they also affect the unconformably overlying Meson Group. The Cañani pluton abuts the cleaved Puncoviscana Formation at an angle, yet locally has a very weak foliation, defined by aligned hornblende and biotite (Fig. 5B), suggesting it may have intruded late-syntectonically. However, the granodiorite to quartz diorite phase is relatively fresh and shows no evidence for low-grade metamorphism other than some very minor alteration of biotite to chlorite. Plagioclase shows little or no evidence for intracrystalline strain and/or recrystallization. The weak foliation thus probably is magmatic and hence this pluton intruded after the main phase of Tilcarian folding and foliation development in this part of the Puncoviscana tract. The Meson Group demonstrably unconformably overlies the intrusion along the Cañani Brook, showing that the pluton is older than the Middle Cambrian. Five samples were collected for petrography and geochemistry of the different facies described. One sample of the biotite-hornblende granodiorite was selected for U–Pb SHRIMP and TIMS geochronology.

2.3.2. Tastil granodiorite

The Tastil granodiorite forms part of a large composite pluton that intruded into the Puncoviscana Formation west of Salta (Fig. 1 – Locality 4). Its intrusive relationships are extremely well exposed (Fig. 5C) and hence, its relationships to regional structures could be established. The intrusion cuts foliated and hornfelsed Puncoviscana Formation rocks, but is itself also foliated locally and crosscutting apophyses extending from the pluton into the host are deformed into tight ptygmatic folds (Fig. 5C). In addition, white porphyroblasts (andalusite?) occurring in the hornfelsed aureole were deformed and aligned in the foliation, suggesting the granodiorite intruded syntectonically during deformation. Matteini et al. (2008) and Hausser et al. (2011) reported a Laser Ablation ICPMS-MC U–Pb age of 534 ± 7 Ma for this phase of the batholith. Hongn et al. (2010) reported a U–Pb TIMS zircon age of 526 ± 1.3 Ma for a younger cross-cutting dacite porphyry phase, which we consider a minimum age of the granodiorite phase. They also presented an age of 517 ± 2 Ma for the red granite, which represents the youngest phase of this pluton. The reported laser ablation ICPMS-MC U–Pb zircon age of 534 ± 7 Ma (Hausser et al., 2011) overlaps in error with the U–Pb TIMS age of the dacite porphyry, suggesting the age difference between these two phases could be less pronounced. Considering the slightly peraluminous nature of the granodiorite, the dated magmatic-looking zircons could be inherited in part from the host Puncoviscana Formation, which contains magmatic zircons of this age in tuffaceous beds (see below).

2.4. Arequipa-Antofalla block

The Arequipa-Antofalla block comprises a Proterozoic, ribbon-like crustal terrane, exposed along the central part of the present-day Andean margin (Fig. 3) This block is critical for understanding of the pre-Andean history of this part of South America. It was previously considered to be autochthonous (Dalmayrac et al., 1980) and part of Amazonia or a suspect terrane (Coira et al., 1982; Monger et al., 1982; Ramos, 1986; Loewy et al., 2004; Rapela et al., 2007). Loewy et al. (2004) divided this block in: (i) a northern Early- to Mesoproterozoic domain, exposed in southern Peru and western Bolivia, (ii) a central Mesoproterozoic domain in northernmost Chile and (iii) a southern domain in northern Chile and northwestern Argentina that mainly comprises Ordovician rocks. Ramos (2008) on the other hand, considered the Arequipa and Antofalla terranes as two separated blocks.

In the Puna of northwestern Argentina, the southern domain of the Antofalla terrane is mainly covered by Tertiary and Quaternary volcanic rocks; exposures of basement are scarce. However, in the western part of the Puna, several occurrences of metamorphic rocks of greenschist to upper amphibolite facies have been recognised previously (Segerstrom and Turner, 1972; Allmendinger et al., 1982; Viramonte et al., 1993; Hongn, 1994; Becchio et al., 1999). They consist of metasediments and orthogneisses of granitoid composition and have a well-developed north-south-trending foliation. Nd–Sm mineral isochron ages of 525 ± 10 Ma at Mejillones; 509 ± 1 Ma at Salar de Hombre Muerto; and 505 ± 6 Ma at Quebrada Choja, north of Sierra Moreno (Fig. 3) provide some constraints on the age of the peak amphibolite facies metamorphic conditions. These Early to Middle Cambrian ages broadly correspond to the final stages of the Pampean orogenic cycle (Aceñolaza and Toselli, 1981), and suggest a tectonic relationship to Tilcarian deformation and metamorphism in the adjacent Puncoviscana tract. Casquet et al. (2008) presented U–Pb zircon evidence that rocks of the Arequipa-Antofalla block in the Sierra de Maz in western Argentina also experienced a Pampean overprint.

We investigated and sampled orthogneisses of unknown age for U–Pb zircon geochronology, petrography and geochemistry to the west of the Antofalla salt flats, at Cerro Negro (Fig. 1 – locality 7). The othogneiss is an intensely foliated granodiorite containing metamorphic and/or recrystallised quartz, feldspar biotite and muscovite.

3. Existing models of the Puncoviscana Formation

Several hypotheses have been proposed for the origin and evolution of the Puncoviscana Formation, mainly based on recent U–Pb zircon LA-ICP-MC data and whole rock geochemistry.

(i) Kraemer et al. (1995), Keppie and Bahlburgh (1999) and latter Zimmermann (2005), in part based on geochemical data, favoured a foreland basin setting, largely derived from a Pampean fold and thrust belt to the east.

(ii) Jezek et al. (1985) and Adams et al. (2008, 2010), mainly based on sedimentological and detrital zircon studies, proposed that the Puncoviscana Formation formed part of a Gondwanan passive margin, which was not directly associated with consanguineous orogenic activity. The detrital zircon age patterns defined three major groups: Paleoproterozoic-Mesoproterozoic (2400–1400 Ma), late Mesoproterozoic-early Neoproterozoic (1150–850 Ma) and late Neoproterozoic-early Cambrian (650–515 Ma). The main provenance area was interpreted to be the Amazonian shield and Brasiliano belt in Brazil. Schwartz et al. (2008) also favour a passive margin setting for the Puncoviscana Formation.

(iii) Ramos (2008) and Omarini et al. (1999) proposed formation of the Puncoviscana basin as a result of rifting between the Pampia and the Anatofalla terranes, synchronous with the opening of the Chiquitos-Tucavaca aulacogen (between 700 and 535 Ma; Ramos et al., 2000) and separation of Antofalla from Arequipa. The basin was closed during the Pampean orogenic cycle by east-directed subduction, reattaching Antofalla to Pampia. The Puncoviscana Formation was assembled into an accretionary complex during this event.

(iv) Collo et al. (2009) also proposed a rift-related basinal setting, but now between a 640 and 600 Ma east-facing Cordoba Arc of Escayola et al. (2007) in the east and the Pampia terrane in the west. Rifting never evolved to seafloor spreading.

(v) Rapela et al. (2007) proposed that the Puncoviscana Formation and Eastern Pampean belt represent the same sedimentary basin (although they did not specify what type of basin) and

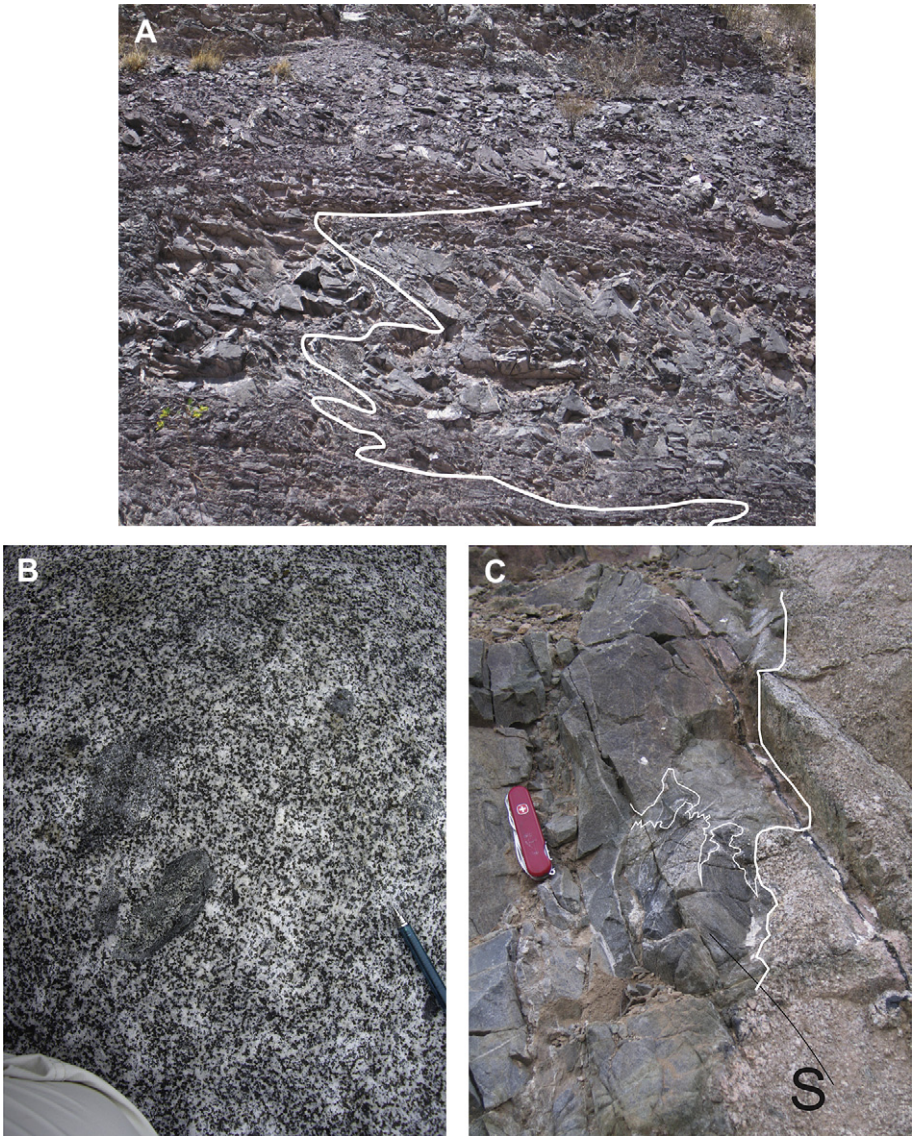

Fig. 5. (A) Large tight to isoclinal early recumbent folds in a subvertical cliff in the Quebrada de Huamahuaca. The recumbent folds fold and crenulate an older cleavage. The vertical width of the photo is approximately 2.5 m. Such structures have not been observed in the Meson Group B. Cañani biotite-hornblende quartz diorite with mafic enclaves in Cañani Brook, near contact with unconformably overlying Meson Group. Note that the hornblende locally has a weak alignment parallel to pencil. (C) Contact between Tastil granodiorite and Puncoviscana Formation hornfelsed in its aureole. The granodiorite contact appears to have been folded conform structures present in the host rock and has a moderate to weak foliation at its margin. Small apohyses (marked in white) of the granodiorite have been buckled into ptygmatic folds.

are correlative sedimentary successions of the Saldana Belt deposited along the southern margin of the Kalahari craton (provenance from the Dom Feliciano-Gariep orogen (Fig. 3) and the EAAO, East African Antarctic Orogen)

4. Analytical methods

4.1. U–Pb geochronology

Heavy mineral concentrates from our samples were prepared using standard crushing, grinding, Wilfley™ table and heavy liquid mineral separation techniques at the Geological Survey of Canada (GSC). These were followed by separation of zircon grains using a Frantz™ isodynamic separator and hand picking. Grains were selected in order to maximize the variety of grain morphologies, and as such, do not represent statistically representative morphological populations.

Zircon grains from samples VLE07-104, VLE07-109, VLE07-126, VLE07-113 and VLE07-04 and fragments of the GSC laboratory zircon standard (z6266; $^{206}Pb/^{238}U$ age = 559 Ma) were cast in an epoxy mount (mount GSC IP#522), polished with diamond compound to reveal the grain centers, and photographed in transmitted light. The zircon crystals were imaged using a Zeiss Evo 50 scanning electron microscope (SEM) with both back-scattered electron (BSE) and cathodoluminescence (CL) imaging to reveal internal features of the zircon grains. U–Pb analyses were obtained on zircons using the sensitive high-resolution ion microprobe

Table 1
Major and trace elements geochemistry.

Sample	SiO_2	Al_2O_3	Fe_2O_3(T)	MnO	MgO	CaO	Na_2O	K_2O	TiO_2	P_2O_5	LOI	Total
VLE 07 E 100	48.93	15.86	14.5	0.202	7.14	1.42	2.37	1.08	1.579	0.14	6.04	99.26
VLE 07 E 103	74.05	10.08	3.76	0.073	1.65	1.23	1.97	2.08	0.498	0.16	2.83	98.38
VLE 07 E 104	53.62	24.56	5.19	0.031	2.13	0.11	0.58	9.37	0.367	0.06	4.39	100.4
VLE 07 E 107	73.21	11.62	4.45	0.04	1.79	0.33	2.31	2.5	0.639	0.19	2.13	99.22
VLE 07 E 108	64.09	16.91	6.15	0.067	3.1	0.26	0.04	5.56	0.729	0.19	3.84	100.9
VLE 07 E 109	68.71	13.52	3.61	0.029	1.19	0.64	2.34	3.47	0.665	0.22	2.57	96.95
VLE 07 E 04	76.26	8.73	2.87	0.06	0.8	2.33	1.85	1.74	0.442	0.14	3.21	98.44
VLE 07 E 113	60.28	15.62	7.02	0.118	3.1	5.71	2.46	2.58	0.683	0.15	1.31	99.03
VLE 07 E 126	70.24	12.51	1.81	0.029	1.85	0.14	0.84	4.36	0.208	0.06	3.2	95.23
VLE 07 E 105	52.22	23.88	5.83	0.038	2.28	0.18	0.07	9.25	0.506	0.03	4.68	98.96

Sample	Sc	Be	V	Co	Ni	Cu	Zn	Ga	Ge	As	Rb	Sr
VLE 07 E 100	54	2	366	50	40	40	250	21	1.8	8	48	47
VLE 07 E 103	8	2	55	9	<20	<10	70	13	1.4	17	90	45
VLE 07 E 104	13	6	89	6	<20	<10	50	36	2	<5	410	36
VLE 07 E 107	9	2	70	10	<20	<10	50	14	1.2	9	101	42
VLE 07 E 108	14	5	99	14	30	<10	100	26	2.4	<5	235	16
VLE 07 E 109	9	3	76	8	<20	<10	40	17	1.4	10	136	48
VLE 07 E 04	6	2	43	6	<20	20	50	10	1.3	48	73	46
VLE 07 E 113	20	3	155	19	<20	40	<30	17	1.3	8	99	277
VLE 07 E 126	5	3	14	4	<20	30	60	17	1.3	8	154	36
VLE 07 E 105	10	7	161	7	<20	20	60	42	2.3	97	427	9

Sample	Y	Zr	Nb	Mo	Ag	In	Sn	Sb	Cs	Ba	La	Ce
VLE 07 E 100	45.1	123	4.5	<2	<0.5	<0.1	1	<0.2	1.2	163	13.9	32
VLE 07 E 103	18.8	160	9.1	2	<0.5	<0.1	4	1.6	3.1	251	24.3	54.6
VLE 07 E 104	64	367	21.1	<2	<0.5	0.1	9	<0.2	13.6	963	78.2	168
VLE 07 E 107	23.6	287	11.6	2	<0.5	<0.1	6	1.3	3.4	270	38	82.1
VLE 07 E 108	41.6	235	19.3	<2	<0.5	<0.1	5	0.6	8.6	530	56	114
VLE 07 E 109	30.4	260	11.6	<2	<0.5	<0.1	4	1.9	3.9	305	43.2	93.2
VLE 07 E 04	24.4	245	8.3	3	<0.5	<0.1	1	<0.2	3.6	286	27	55.2
VLE 07 E 113	24	159	9.5	3	<0.5	<0.1	6	1.7	4.7	436	27.4	59.8
VLE 07 E 126	28.6	159	12.7	<2	<0.5	<0.1	6	2	10.8	319	43.9	96.2
VLE 07 E 105	125	905	39.7	<2	<0.5	0.2	17	0.4	15.5	1057	64.4	135

Sample	Pr	Nd	Sm	Eu	Gd	Tb	Dy	Ho	Er	Tm	Yb	Lu
VLE 07 E 100	4.05	17.1	4.5	1.39	5.97	1.09	7.17	1.58	4.83	0.721	4.53	0.675
VLE 07 E 103	6.01	20	4.18	0.776	3.52	0.6	3.57	0.7	2.02	0.291	1.89	0.297
VLE 07 E 104	18.7	64.6	13.8	2.3	12.7	2.04	12.4	2.52	7.39	1.07	6.59	0.95
VLE 07 E 107	9.12	30.5	5.99	1.05	4.43	0.72	4.22	0.83	2.46	0.367	2.4	0.353
VLE 07 E 108	11.6	40.7	8.93	1.55	7.73	1.15	6.86	1.42	4.24	0.641	4.09	0.596
VLE 07 E 109	10.4	35.2	6.97	1.28	5.22	0.99	5.38	1.06	3.07	0.458	2.82	0.401
VLE 07 E 04	6.23	21.6	4.59	0.895	4.31	0.71	4.01	0.81	2.5	0.375	2.4	0.354
VLE 07 E 113	6.73	23.3	4.96	1.1	3.88	0.67	4.15	0.84	2.45	0.358	2.35	0.345
VLE 07 E 126	10.8	36.4	7.14	0.791	4.98	0.92	5.56	1.09	3.21	0.488	3.2	0.466
VLE 07 E 105	14	56.8	13.3	1.96	14.5	2.83	19.2	4.35	13.6	2.13	13.8	1.96

Sample	Hf	Ta	W	Tl	Pb	Bi	Th	U	Cr2O3	CuO	NiO
VLE 07 E 100	3.5	0.36	<0.5	0.62	19	1.9	4.36	1.11	0.02	0.005	0.013
VLE 07 E 103	3.9	0.79	2	0.66	<5	1	8.68	2.15	0.02	0.004	<0.004
VLE 07 E 104	12.5	2.72	<0.5	4.03	<5	2.2	46.4	8.16	<0.01	<0.002	<0.004
VLE 07 E 107	6.7	0.98	2.6	0.57	<5	0.9	11.1	2.76	0.02	<0.002	<0.004
VLE 07 E 108	5.6	1.56	0.7	1.59	<5	0.8	14.4	3.51	0.01	<0.002	0.005
VLE 07 E 109	6.1	1.03	3.3	0.83	<5	0.8	11.1	2.56	0.02	<0.002	<0.004
VLE 07 E 04	6.5	0.83	0.8	0.57	8	0.8	9.22	2	0.01	0.003	<0.004
VLE 07 E 113	4.1	0.87	1.4	0.15	<5	0.2	9.87	3.01	0.01	0.005	<0.004
VLE 07 E 126	4.7	1.25	1.5	1.1	11	1.9	15.9	4.55	<0.01	0.004	<0.004
VLE 07 E 105	22.5	4.32	<0.5	2.73	7	46.5	42.1	8.68	<0.01	0.003	<0.004

Table 2
Summary of shrimp U–Pb data from sample VLE07-104.

Spot name	ppm U	ppm Th	ppm Rad 206	$^{232}Th/^{238}U$	% err	Total $^{206}Pb/^{238}U$	% Err	Total $^{208}Pb/^{232}Th$	% Err	204corr $^{206}Pb/^{238}U$ Age	1 err	207corr $^{206}Pb/^{238}U$ Age
9578-1.1	542	666	40.1	1.27	0.18	0.086	1.1	0.0261	1.9	533	6	533
9578-1.2	388	134	29.2	0.36	0.37	0.088	1.1	0.0284	3.4	542	6	543
9578-3.1	136	74	10.0	0.57	0.48	0.086	1.3	0.0302	4.3	530	7	529
9578-2.1	494	97	57.0	0.20	0.95	0.134	1.1	0.0637	2.7	812	8	785
9578-9.1	181	128	13.3	0.73	0.36	0.086	1.2	0.0282	3.5	531	6	531
9578-11.1	186	101	13.9	0.56	0.41	0.087	1.2	0.0291	3.8	539	6	536
9578-15.2	231	115	17.2	0.52	0.38	0.087	1.2	0.0287	3.5	535	6	536
9578-16.1	125	40	9.2	0.33	1.19	0.086	1.3	0.0296	5.9	531	7	528
9578-22.1	473	616	36.1	1.35	0.17	0.089	1.1	0.0287	1.8	548	6	548
9578-23.1	390	422	29.6	1.12	0.21	0.088	1.1	0.0284	2.1	545	6	546
9578-26.1	208	225	15.9	1.12	0.39	0.088	1.2	0.0279	2.8	549	6	546
9578-33.1	326	202	24.8	0.64	0.41	0.088	1.1	0.0276	2.8	546	6	545
9578-41.1	234	190	17.3	0.84	0.30	0.086	1.2	0.0267	2.9	532	6	532
9578-48.1	265	177	20.2	0.69	0.32	0.089	1.2	0.0276	3.0	548	6	546
9578-16.1_A	121	32	8.8	0.28	0.71	0.084	1.3	0.0307	6.3	523	7	521
9578-22.1_A	483	624	36.1	1.33	0.24	0.087	1.1	0.0281	1.9	538	6	537
9578-23.1_A	402	434	29.6	1.11	0.21	0.086	1.2	0.0270	2.2	530	6	529

Errors are 1 unless otherwise specified.

(SHRIMP II) at the Geological Survey of Canada (Ottawa). Full analytical details of the U–Pb analyses are presented in Table 7. Analyses were conducted using an ^{16}O-primary beam, projected onto the zircons at 10 kV. The sputtered area used for analysis was ~18 μm some small cores were re-analyzed with 9 um spot with a beam current of ~10 nA. The count rates at ten masses including background were sequentially measured over six scans with a single electron multiplier and a pulse counting system with deadtime of 27 ns. Off-line data processing was accomplished using SQUID 2.22.08.04.30 (rev. 30 Apr 2008). The 1 sigma external errors of $^{206}Pb/^{238}U$ ratios reported in the data table incorporate a ±1.1% error in calibrating the standard zircon (see Stern and Amelin, 2003). No fractionation correction was applied to the Pb isotopic data; common Pb correction utilized the Pb composition of the surface blank. The ^{207}Pb method was used to calculate $^{206}Pb/^{238}U$ ages and errors. Isoplot v. 3.00 (Ludwig, 2003) was used to generate concordia plots and calculate weighted means. The error ellipses on the Concordia diagram and the weighted mean errors are reported at 2 sigma.

U–Pb TIMS analytical methods utilized in this study are outlined in Parrish et al. (1987) and Davis et al. (1996) and references therein. Grains were handpicked and grouped on basis of morphology and clarity. Multigrain zircon fractions analyzed were very strongly air abraded. Multigrain fractions of titanite were lightly air abraded. Treatment of analytical errors follows Roddick et al. (1987) with errors on the ages reported at the 2σ level. Procedural blank values for this study ranged from 0.1 to 0.2 pg U and 2–10 pg Pb for zircon analyses, 1–2 pg U and 7–11 pg Pb for titanite analyses and 0.1 pg U and 1–2 pg Pb for monazite analyses.

4.2. Pb–Pb isotopes

LA-ICPMS-MC Pb–Pb analyses were carried out in the Geochronology Laboratory of the Geological Survey of Canada (Ottawa) as part of an ongoing experimental research performing Pb–Pb analysis with Laser Ablation techniques. Determination of the initial lead isotopic composition of old rocks is hampered by the mobility of uranium, especially in the near surface weathering environments. Disturbance of the U/Pb ratio hampers calculation of initial lead isotopic ratios by extrapolation from the measured present day lead isotopic compositions. K-feldspars is typically characterized by very low U/Pb ratios and as such is expected to accumulate little radiogenic lead over the history of the rock. Hence, the lead isotopic composition of alkali feldspar is typically rather insensitive to late uranium mobility and should be similar to the initial lead isotopic composition of the system (Gariepy and Allegre, 1985; Housh and Bowring, 1991). However, previous studies have demonstrated that the lead isotopic compositions of feldspar could be more radiogenic than those of the associated sulfides which are also presumed to record the initial lead isotopic composition of the magmatic system. We applied the experimental procedures of stepwise removal of lead through vacuum volatilization and HF leaching of the alkali feldspars to remove the radiogenic lead (Gariepy and Allegre, 1985; Manhes et al., 1980), followed by analysis of the Pb–Pb isotopic composition of K-feldspars with LA-ICP-MS-MC in epoxy mounts to determine the initial lead isotopic composition of the rocks. In addition, the Pb–Pb isotopic composition of feldspars previously analyzed by conventional TIMS methods (samples 216-87, 218-87, 218-88, 219-88, 37-89, 78 of Davis et al., 1996) were also analyzed by LA-ICPMS-MC, together with our sample VLE07-113, for use as internal standards.

After crushing the alkali feldspar crystals were crushed and sieved and bulk feldspars separates were prepared from 100 to 200 μm fractions by heavy liquids (2.58 g/cm^3) and a Frantz magnetic separator. Following this the alkali feldspars crystals were handpicked from sample VLE07-113 and used as internal standards.

A part of the light fraction (K-feldspars) was handpicked to separate possible fragments of quartz or albite. A fraction of crystals was separated to be analyzed without leaching and a second fraction was leached following the procedure described by Davis et al. (1996). Few crystals of the more clean appearance of each fraction of sample VLE07-113 and internal standards were selected and mounted in two epoxy mounts and polished for imaging using a Zeiss Evo 50 scanning electron microscope (SEM) with back-scattered electron (BSE) to detect any crystal anisotropy or perthite intergrowth in the crystals. Both non-leached crystals and leached crystal mounts were analyzed for Pb–Pb with using a Thermo-Fisher Neptune MC-ICP-MS coupled with a Nd:YAG UP213 New Wave Laser Ablation system. Radiogenic and common lead concentrations were compared, results obtained in both fractions (leached and not leached) were equivalent and data for sample VLE07-113 from Cañani granodiorite are presented in Table 8.

5. Sample descriptions and results

5.1. Puncoviscana Formation at Puncoviscana locality

We collected a felsic tuff (VLE07-104) and wacke (VLE07-109) bed of the Puncoviscana Formation in the village of Puncoviscana (Fig. 2B). The sample locality is situated at 22°14′ 57.4″S and 64° 58′ 07.7″ W

(Fig. 2 and outcrop photograph in Fig. 3B). The felsic tuff bed was ca. 15 cm and the wacke bed ca. 50 cm thick. The felsic tuff contains quartz phenocrysts in a very fine-grained, strongly foliated matrix of white mica and does not contain any detrital mineral clasts such as in the interlayered wacke, leaving little doubt this is a volcanic bed .

5.1.1. Sample VLE07-104

One hundred and eighty five grains were selected from the rhyolitic tuff for analysis. The zircons are clear and commonly have growth zoning. They have oblate to elongate, subhedral to euhedral prismatic morphologies; elongate prismatic crystals are most common. The cores and rims of 60 zircons were analyzed by the U–Pb SHRIMP method (Table 2). The results yielded a $^{206}Pb/^{238}U$ weighted average age of 536.0 ± 5.3 Ma, with minor Neoproterozoic (723–800 Ma), Mesoproterozoic (1.4–1.5 Ga) and Paleoproterozoic (2.4 Ga) cores (Fig. 6a). Five elongated prismatic and transparent grains were selected for single grain TIMS analysis (Table 7), they produced a concordia age of 537.3 ± 0.9 Ma, which we interpreted as the crystallization age of the rhyolitic tuff (Fig. 6b).

5.1.2. Sample VLE07-109

Ninety six zircons were selected for analysis, two populations are present: a group with oblate short prismatic morphologies and a small group charcterised by prismatic clear elongated crystals. Some of the oblate crystals show irregular zoning typical of zircons in mafic igneous rocks. The prismatic zircon grains mainly display regular growth zoning. The cores and rims of sixty eight grains were analyzed by the U–Pb SHRIMP method (Table 3; Fig. 6c, d). The detrital zircon population is dominated by Neoproterozoic zircons with the most prominent peaks at 608 and 777 Ma respectively. The youngest zircon is 569 Ma. Mesoproterozoic zircons have a prominent peak at 1.029 Ga and subsidiary peaks at 1.134, 1.4 and 1.5 Ga. Early Proterozoic grains range between1.65 and 2.4 Ga. There are also some Archean grains at 2.7–2.8 Ga. There is an age gap between the Archean and the oldest Early Proterozoic age (ca. 2.4 Ga).

5.2. Puncoviscana Formation at Quebrada de Humahuaca

We collected a yellowish to light green ca 30 cm thick tuffaceous sandstone bed (VLE 126) with a thickness of circa 50 cm at Purmamarca (23°43′12.5″S, 65°27′ 57.5″W). The tuffaceous bed resembles the felsic tuffs of the Puncoviscana type locality and is interlayered with typical green wacke beds and finer grained red and green siltstones (Fig. 3A).

5.2.1. Sample VLE07-126

Eighty three grains were selected for analyses. The zircons are clear, predominantly elongate and prismatic, and display growth zoning. The cores and rims of 47 grains were analyzed by the U–Pb SHRIMP method. The results are presented in Table 4. The data form a nearly unimodal distribution with a predominant

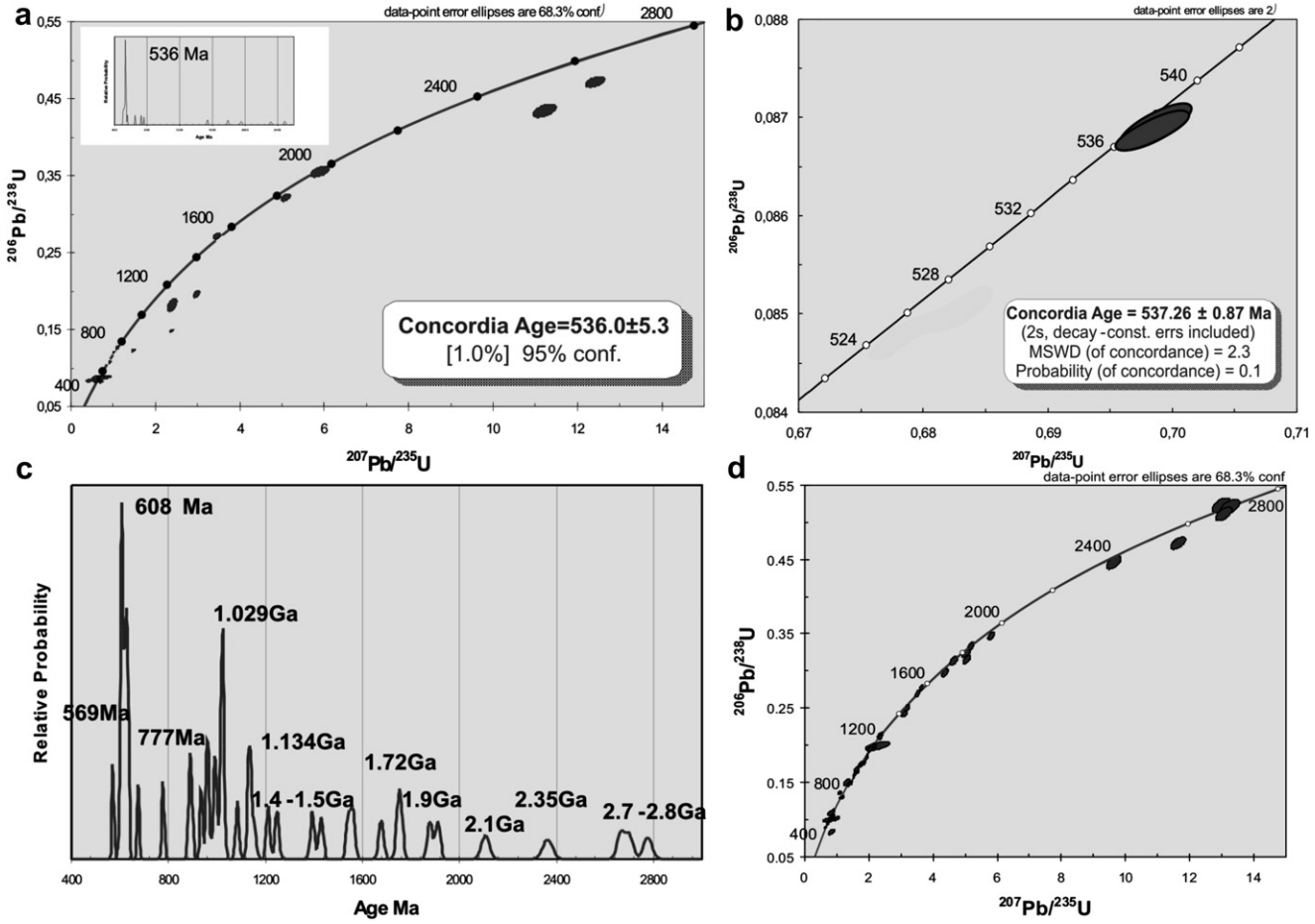

Fig. 6. U–Pb zircon geochronological results for rocks of Puncoviscana Formation, at Puncoviscana locality. Concordia diagrams and probability density plots are shown. In the probability density plot diagram the $^{207}Pb/^{206}Pb$ and the $^{238}U/^{206}Pb$ ages have been used for zircons older and younger than 900 Ma, respectively: (a) sample VLE07-104, felsic tuff, U–Pb SHRIMP concordia diagram, (b) sample VLE07-104, felsic tuff, U–Pb TIMS concordia diagram, (c) probability density plot diagram of sample VLE07-109 andesitic–basaltic volcaniclastic rocks, (d) sample VLE07-109 andesitic–basaltic volcaniclastic rocks U–Pb SHRIMP data concordia diagram.

Table 3
Summary of shrimp U–Pb data from sample VLE07-109.

Spot name	ppm U	ppm Th	ppm Rad 206	$^{232}Th/^{238}U$	% err	Total $^{206}Pb/^{238}U$	% Err	Total $^{208}Pb/^{232}Th$	% Err	204corr $^{206}Pb/^{238}U$ Age	1 err	207corr $^{206}Pb/^{238}U$ Age
9579-1.2	546	44	162.4	0.08	0.67	0.346	1.1	0.1072	3.3	1917	18	1906
9579-4.1	89	88	11.4	1.01	0.47	0.148	1.5	0.0490	3.6	892	12	890
9579-4.2	204	109	17.3	0.55	0.44	0.099	1.3	0.0315	4.0	608	8	609
9579-5.1	305	70	25.7	0.24	0.55	0.098	1.2	0.0338	4.7	603	7	604
9579-6.1	279	352	79.6	1.30	0.27	0.332	1.1	0.0959	1.7	1847	18	1846
9579-6.2	175	246	47.2	1.46	0.31	0.314	1.2	0.0937	2.9	1761	19	1741
9579-7.1	1310	578	125.6	0.46	0.20	0.112	1.1	0.0341	1.9	682	7	683
9579-8.1	253	67	58.2	0.27	0.56	0.268	1.1	0.0821	3.2	1531	16	1531
9579-8.2	414	101	98.0	0.25	0.47	0.276	1.1	0.0784	2.7	1570	15	1573
9579-10.1	194	91	26.9	0.49	0.49	0.162	1.3	0.0562	3.4	967	11	967
9579-10.2	203	41	27.9	0.21	0.74	0.160	1.3	0.0490	5.2	957	11	957
9579-11.1	430	128	57.5	0.31	0.41	0.156	1.1	0.0477	3.0	933	10	931
9579-11.2	81	1	7.0	0.01	5.98	0.100	1.7	0.1278	27.6	618	11	609
9579-12.1	165	108	23.3	0.68	0.45	0.164	1.3	0.0506	3.3	979	12	977
9579-14.1	278	183	24.6	0.68	0.35	0.103	1.2	0.0344	3.0	633	7	633
9579-15.1	156	74	28.5	0.49	0.55	0.213	1.3	0.0699	3.4	1241	14	1242
9579-15.2	183	64	32.9	0.36	0.57	0.210	1.2	0.0675	4.9	1226	14	1225
9579-19.1	170	79	25.2	0.48	0.52	0.174	1.3	0.0552	3.6	1030	12	1028
9579-20.1	156	53	13.9	0.35	0.87	0.105	1.4	0.0449	4.8	633	9	632
9579-20.2	199	133	15.1	0.69	0.40	0.089	1.4	0.0274	3.9	546	7	548
9579-21.1	114	67	51.2	0.60	0.58	0.522	1.2	0.1512	2.6	2707	27	2735
9579-21.2	82	50	31.2	0.63	0.65	0.446	1.3	0.1420	3.8	2372	26	2355
9579-22.1	128	42	18.3	0.34	0.71	0.167	1.4	0.0493	5.0	995	13	996
9579-23.1	128	44	10.9	0.35	0.73	0.100	1.5	0.0342	6.3	607	9	611
9579-23.2	84	26	7.1	0.32	0.91	0.100	1.7	0.0384	7.2	605	11	609
9579-23.3	229	77	19.7	0.35	0.54	0.101	1.3	0.0331	4.6	617	8	615
9579-25.1	44	30	5.7	0.70	0.85	0.150	1.9	0.0549	5.9	894	16	899
9579-30.1	225	55	34.0	0.25	0.62	0.176	1.2	0.0531	5.7	1045	12	1041
9579-33.1	194	100	21.4	0.54	0.46	0.129	1.3	0.0442	3.5	780	10	779
9579-36.1	227	104	28.4	0.48	0.45	0.146	1.2	0.0479	3.3	877	10	876
9579-39.1	55	20	9.3	0.38	1.04	0.200	1.7	0.0680	6.4	1164	21	1157
9579-39.2	145	74	24.0	0.53	0.55	0.194	1.3	0.0598	3.7	1137	14	1138
9579-42.1	316	421	27.0	1.38	0.24	0.100	1.2	0.0326	2.3	611	7	612
9579-42.2	210	244	17.8	1.20	0.33	0.099	1.4	0.0313	3.2	607	8	608
9579-47.1	129	52	21.9	0.42	0.64	0.198	1.3	0.0654	4.0	1166	14	1163
9579-51.1	424	318	36.2	0.77	0.26	0.099	1.2	0.0316	2.4	610	7	609
9579-52.1	258	122	38.8	0.49	0.43	0.175	1.2	0.0550	3.0	1039	11	1037
9579-53.1	133	148	11.1	1.15	0.36	0.098	1.4	0.0310	3.4	600	8	599
9579-53.2	401	163	34.4	0.42	0.75	0.100	1.3	0.0347	4.2	613	8	614
9579-58.1	90	58	24.3	0.67	0.60	0.313	1.3	0.0937	3.3	1754	21	1752
9579-60.1	129	39	27.6	0.31	0.70	0.249	1.3	0.0769	4.0	1434	16	1428
9579-62.1	61	77	27.3	1.30	0.51	0.520	1.4	0.1454	2.5	2696	30	2695
9579-63.1	536	234	148.7	0.45	0.43	0.324	1.1	0.0989	2.5	1803	18	1797
9579-64.1	19	21	1.4	1.14	0.96	0.083	3.0	0.0361	8.2	510	15	499
9579-67.1	131	145	57.6	1.14	0.37	0.510	1.2	0.1469	1.9	2658	26	2635
9579-67.2	514	296	207.7	0.60	0.49	0.472	1.2	0.1497	2.2	2487	24	2425
9579-71.1	178	154	28.1	0.89	0.35	0.184	1.2	0.0564	2.5	1087	12	1084
9579-73.1	247	114	51.2	0.48	0.41	0.241	1.1	0.0765	2.5	1392	14	1383
9579-76.1	406	104	35.3	0.26	0.43	0.101	1.2	0.0306	3.8	622	7	622
9579-79.1	257	152	20.6	0.61	0.36	0.094	1.2	0.0318	3.2	575	7	576
9579-85.1	110	69	12.8	0.65	0.52	0.136	1.4	0.0430	4.0	816	11	822
9579-86.1	293	141	43.3	0.50	0.38	0.172	1.2	0.0571	2.6	1024	11	1025
9579-88.1	34	27	3.1	0.82	0.86	0.109	2.2	0.0344	7.4	660	14	664

Errors are 1 unless otherwise specified.

population at 536.4 ± 5.3 Ma, which confirms the tuffaceous character of the bed. It has minor subsidiary peaks at 1.4 and 1.8 Ga (Fig. 7a).

5.3. Cañani pluton: granodiorite to quartz diorite phase (VLE07-113)

5.3.1. U–Pb geochronology

The analyzed sample was collected along Cañani Brook (22° 20′ 04.8″S and 64°52′ 02.4″W), 15 km to the southeast of Santa Victoria Oeste. Eighty one grains were selected for analyses. Zircons display growth zoning and are euhedral, prismatic, transparent and clear. The cores and rims of 22 zircon grains were analyzed by U–Pb SHRIMP (Table 5). The zircon grains yielded a $^{206}Pb/^{238}U$ weighted average age of 523 ± 4.7 Ma (Fig. 7e). Two elongated prismatic and transparent grains were selected for single grain TIMS analysis (Table 7). They gave a concordia lower intercept age of 523.7 ± 0.8 Ma, which is interpreted as the crystallization age of the pluton (Table 7).

5.3.2. Pb–Pb isotopes

Twenty five feldspars grains of the granodiorite to quartz diorite phase were selected for LA-ICPMS-MC Pb-Pb isotopic analyses. The analyzed feldspars (four crystals) yield $^{207}Pb/^{204}Pb$ ratios of 15.714–15.746 and $^{206}Pb/^{204}Pb$ ratios of 18.248–18.266 (Table 8). They show high $^{207}Pb/^{204}Pb$ ratios (relative to $^{206}Pb/^{204}Pb$), plotting above Stacey and Kramers (1975) crustal evolution curve coincident with Antofalla Basement in Chile and Argentina and the Western Brazilian Shield field (Loewy et al., 2004 and references therein) (Fig. 7f).

Table 4
Summary of shrimp U–PB data from sample VLE07-126.

Spot name	ppm U	ppm Th	ppm Rad 206	$^{232}Th/^{238}U$	% err	Total $^{206}Pb/^{238}U$	% Err	Total $^{208}Pb/^{232}Th$	% Err	204corr $^{206}Pb/^{238}U$ Age	1 err	207corr $^{206}Pb/^{238}U$ Age
9580-1.1	50	26	3.6	0.53	1.22	0.085	2.4	0.0359	10.4	520	18	517
9580-3.1	256	163	18.9	0.66	0.41	0.086	1.3	0.0279	4.0	532	7	530
9580-6.1	115	69	8.3	0.62	0.67	0.085	2.0	0.0300	6.2	519	11	519
9580-6.2	511	320	39.5	0.65	0.32	0.090	1.2	0.0306	3.0	555	6	554
9580-7.1	93	59	6.8	0.65	0.69	0.085	1.7	0.0321	6.2	526	9	519
9580-11.1	94	92	6.7	1.01	0.73	0.083	2.4	0.0305	7.2	513	12	507
9580-13.1	291	182	21.6	0.65	0.47	0.087	1.4	0.0265	4.6	535	7	535
9580-15.1	380	325	28.1	0.88	0.30	0.086	1.2	0.0238	4.2	531	6	532
9580-19.1	300	143	23.7	0.49	0.38	0.092	1.2	0.0317	3.3	566	7	566
9580-23.1	178	111	13.2	0.64	0.49	0.087	1.4	0.0271	4.6	531	7	533
9580-28.1	296	225	22.0	0.79	0.39	0.087	1.3	0.0290	3.8	536	7	536
9580-35.1	100	67	7.6	0.69	0.53	0.090	1.4	0.0268	5.0	547	8	549
9580-45.1	123	149	9.2	1.25	0.37	0.087	1.4	0.0287	3.5	536	7	534
9580-48.1	52	27	3.9	0.53	0.90	0.091	1.8	0.0305	11.4	545	10	558
9580-48.2	158	77	11.2	0.50	0.53	0.083	1.4	0.0275	5.0	510	7	511
9580-50.1	243	210	18.1	0.89	0.32	0.087	1.2	0.0273	3.1	535	6	539
9580-56.1	209	169	14.9	0.83	0.54	0.084	1.7	0.0290	5.0	512	9	518
9580-58.1	134	106	9.5	0.81	0.46	0.084	1.5	0.0295	4.3	511	8	515
9580-56.1_A	175	135	11.9	0.80	0.62	0.081	1.8	0.0283	7.4	491	9	495
9580-58.1_A	97	74	6.8	0.79	0.61	0.082	1.8	0.0292	5.6	509	9	509
9580-61.1	653	52	45.2	0.08	0.54	0.081	1.1	0.0292	5.0	500	5	498
9580-62.1	135	63	10.0	0.48	1.19	0.087	1.4	0.0270	5.0	533	7	533
9580-67.1	118	73	8.7	0.64	0.87	0.086	1.5	0.0310	4.6	530	8	533
9580-67.2	282	132	20.7	0.48	0.37	0.086	1.2	0.0269	5.1	529	6	530

Errors are 1 unless otherwise specified.

5.4. Cerro Negro orthogneisses – Antofalla southern Domain (VLE07-04)

The selected sample was collected to the west of Antofalla salt flat (25° 49′ 13.65″S and 67° 50′ 59.87″W). Two hundred and forty two zircon grains were selected for analyses, the selected zircons are euhedral, prismatic, transparent, clear and display growth zoning. Seventy four zircon grains (cores and rims) were analyzed by U–Pb SHRIMP. Our analyses (Table 6) show a main zircon population and a Cambrian concordia age of 523 ± 0.7 Ma, which we interpret as the age of the intrusion (Fig. 7b). Populations with ages of 654 Ma, 875 Ma, 940 Ma, 1040 Ma, 1175 Ma, 1392 Ma, 1500 Ma, 1681 Ma and 1881 Ma were measured in the inherited cores of the zircons. The Neoproterozoic and Mesoproterozoic (Grenvillian) ages are the most frequent (Fig. 7c).

6. Geochemistry

Major, trace and rare earth element compositions of the Puncoviscana Formation felsic and mafic volcanic rocks, Cañani pluton and Cerro Negro orthogneiss are presented in Table 1. In the village of Puncoviscana, the most mafic sample (SiO_2: 48. 93 wt %) of the Puncoviscana Formation is a basalt or basaltic andesite. The SiO_2: content of the volcanogenic wacke and felsic tuff bed range between 53.62% and 73.21%. The tuffaceous bed sampled in Quebrada de Humahuaca (VLE07-126) has a SiO_2 content of 70.24%. In the Nb/Y–Zr/Ti diagram of Winchester and Floyd (1977) the felsic tuff beds plot in the field of rhyolite (Fig. 8a), the green wacke in the field of andesite and the mafic volcanic layer at the boundary between the basalt and andesite fields. The volcanic rocks have calc-alkaline to high K calc-alkaline signatures (Fig. 8b). All samples have similar characteristics, displaying enrichment in light REE and negative Ta, Nb, Sr, P and Ti anomalies on primordial mantle normalized extended trace element diagrams (Fig. 8c). On the Bhatia and Crook (1986) discrimination diagrams (Fig. 4), the wacke samples (VLE 108 and 109) typically plot in the continental island arc and active continental arc fields. The enrichment in Sc and Co in the samples relative to the passive margin fields suggests that the Puncoviscana Formation originally contained unstable volcanic material such as glass and lithic fragments (Bhatia and Crook, 1986), consistent with an epiclastic origin. Our results documented herein are consistent with the geochemical data of the Puncoviscana Formation (Fig. 4) from Zimmerman (2005), indicating an overall arc magmatic source. The SiO_2 content of the Cañani pluton is 60.28% and plot in the field of diorite (Fig. 8). The SiO_2 content of the Cerro Negro orthogneiss is 76.26% and classifies as a granite.

Similar to the volcaniclastic rocks, the intrusive rocks have an enrichment in Light REE and negative Ta, Nb, Sr, P and Ti anomalies (Fig. 8c), implying they all have similar subduction-related signature (Wood et al., 1979). The Tastil granodiorite shows the same geochemical signatures (Hausser et al., 2010). In the Hf/3, Th, Ta discrimination diagram of Wood (1980) all analyzed mafic rocks plot in the Arc-basalt (D) field (Fig. 8d).

The geochemistry of the Puncoviscana Formation suggests that these rocks were epiclastic volcanogenic sediments derived from magmatic sources and as such does not support the passive margin hypothesis of Jezek et al. (1985) and Adams et al. (2008, 2010). Rather the geochemical similarity of the Puncoviscana Formation with the associated coeval volcanic and plutonic rocks supports an arc-related tectonic setting.

7. Age and provenance of the Puncovicana Formation

The age dates presented herein impose tight constraints on the age of deposition and deformation of the Puncoviscana Formation. The youngest zircon measured in our analyzed samples was collected in Quebrada de Humahuaca near Purmamarca, north of Jujuy, in a tuffaceous sandstone bed (VLE07-126), which gave an age of 536.4 ± 5.3 Ma (see above). This age overlaps within error with the 537 ± 0.9 Ma felsic tuff beds near the type locality in the village of Puncoviscana (VLE07-104). In the latter locality, the sampled Puncoviscana Formation occurs in the core of a large NE-trending antiform, which according to Turner (1964), was truncated by steeply west-dipping faults on all sides. Field evidence suggests the faulting history associated with this early structure was complex and polyphase, including a Tilcarian-Pampian (pre-Meson Group) thrusting history (Fig. 2C, D). This part of the Puncoviscana Formation thus may represent an old segment of this unit. Detrital zircons in the green wacke bed interlayered with the tuff beds have prominent Ediacaran peaks of 608 and 569 Ma. Deposition of the

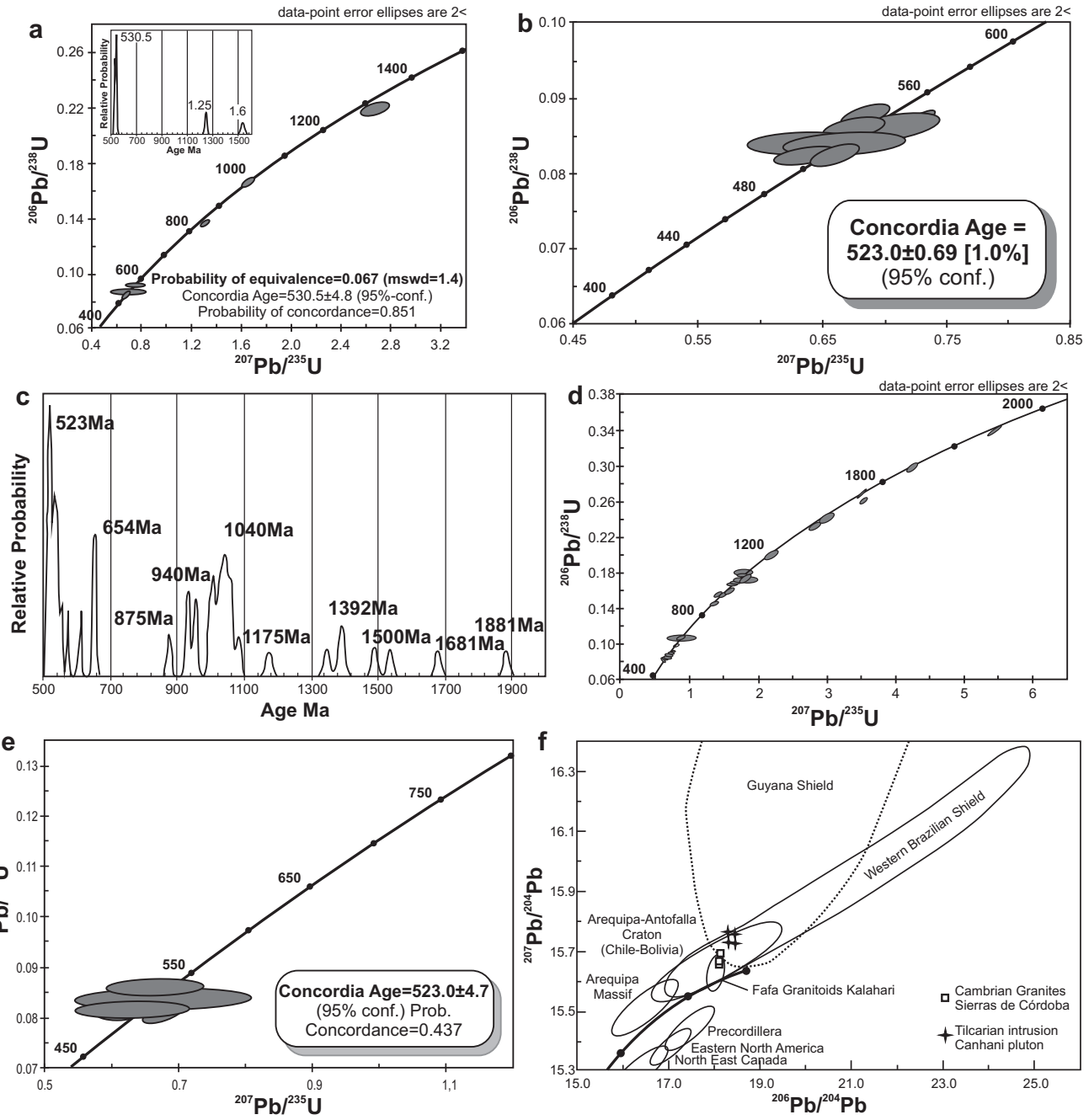

Fig. 7. U–Pb zircon geochronological results for rocks of Puncoviscana Formation at Quebrada de Humahuaca (a), Cañani granodiorite (b) and Cerro Negro (Antofalla) ortogneiss (c, d, e). Concordia diagrams and probability density plots are shown. In the probability density plot diagram the $^{207}Pb/^{206}Pb$ and the $^{238}U/^{206}Pb$ ages have been used for zircons older and younger than 900 Ma, respectively: (a) sample VLE07-126, tuff, U–Pb concodia diagram and probability density plot, (b) sample VLE07-04, Cerro Negro (Antofalla) orthogneiss U–Pb SHRIMP Concordia diagrams, (c) sample VLE07-04, Cerro Negro (Antofalla) orthogneiss U–Pb SHRIMP data probability density plot; (c, d) sample VLE07-113, Cañani granodiorite U–Pb SHRIMP concordia diagram, (f) sample VLE07-113 Cañani granodiorite Pb isotopic diagram comparing major cratonic rocks of South America and eastern North America with Cambrian intrusive Cañani granodiorite and Cambrian granites from Sierras de Córdoba (Schwartz and Gromet, 2004 and references therein).

Puncoviscana Formation thus may have started during the latest Ediacaran (cf. Omarini et al., 1999), but is mainly Early Cambrian rather than Neoproterozoic, consistent with the interpretations of Durand and Aceñolaza (1990). The Puncoviscana Formation was intruded by the late-syn- or post-tectonic (see above) calc-alkaline Cañani pluton (Fig. 5b), which yielded a precise Early Cambrian U–Pb TIMS age of 523.7 ± 0.8 Ma. Pampean–Tilcarian deformation is thus constrained in this part of the Puncoviscana tract between 537 and 524 Ma. Detrital zircon populations of the Puncoviscana Formation published by other workers showed very similar patterns as ours (e.g. Hausser et al., 2011). However, Adams et al. (2008, 2010) measured Early Cambrian zircons as young as 522 ± 4 Ma. and 514 ± 8 Ma near the southwesternmost extent of the Pucoviscana tract. Puncoviscana depocentres thus appear to become younger to the southwest, concomitant with deformation and intrusion of calc-alkaline plutons in the northeast. The

Table 5
Summary of shrimp U–PB data from sample VLE07-113.

Spot name	ppm U	ppm Th	ppm Rad 206	$^{232}Th/^{238}U$	% err	Total $^{206}Pb/^{238}U$	% Err	Total $^{208}Pb/^{232}Th$	% Err	204corr $^{206}Pb/^{238}U$ Age	1 err	207corr $^{206}Pb/^{238}U$ Age
9581-1.1	209	160	14.8	0.79	0.32	0.083	1.2	0.0285	3.0	510	7	510
9581-3.1	154	142	10.8	0.95	0.34	0.082	1.3	0.0265	3.3	507	6	506
9581-4.1	201	211	14.9	1.08	0.28	0.086	1.2	0.0275	2.8	532	6	532
9581-8.1	190	201	13.9	1.09	0.29	0.086	1.2	0.0264	2.9	528	6	529
9581-12.1	77	60	5.7	0.80	0.52	0.086	1.5	0.0277	4.9	534	8	530
9581-14.1	107	74	7.6	0.72	0.47	0.084	1.4	0.0280	4.4	515	7	518
9581-18.1	269	283	19.6	1.09	0.25	0.085	1.2	0.0284	2.4	525	6	524
9581-21.1	201	206	14.5	1.06	0.29	0.085	1.2	0.0283	2.8	519	6	519
9581-23.1	95	85	6.7	0.93	0.51	0.083	1.5	0.0270	4.2	511	8	513
9581-24.1	166	126	11.6	0.78	0.45	0.082	1.4	0.0260	4.4	502	7	504
9581-26.1	162	117	11.5	0.74	0.40	0.083	1.3	0.0279	3.8	511	7	513
9581-35.1	280	241	20.2	0.89	0.30	0.084	1.2	0.0281	2.9	521	6	521
9581-36.1	113	75	8.1	0.69	0.53	0.084	1.5	0.0277	5.0	520	8	519
9581-38.1	50	35	3.6	0.72	0.88	0.085	2.1	0.0321	7.9	510	12	522
9581-39.1	119	95	8.4	0.83	0.45	0.083	1.4	0.0311	4.0	513	7	511
9581-40.1	116	74	8.0	0.65	0.54	0.081	1.5	0.0258	5.2	500	7	500
9581-42.1	78	43	5.4	0.57	0.67	0.082	1.6	0.0320	5.9	504	8	505

Errors are 1 unless otherwise specified.

apparent overlap in age between deposition, deformation and magmatism is highlighted by the Tastil granodiorite, which intruded syntectonically into the Puncoviscana Formation ca. 200 km southwest of the Puncoviscana village (see above). If the 534 ± 7 Ma Laser ICPMS U–Pb age is correct (Hausser et al., 2011), it either leaves very little time between deposition and the onset of Tilcarian deformation, or deposition and deformation are diachronous, becoming progressively younger to the west or southwest. Regardless whether the ca. 534 Ma age is possibly too old (see section on Tastil pluton above) and instead slightly younger (but older than 526 Ma – Hongn et al., 2010), the available age constraints suggest that deposition of the relatively thick pile of turbidites of the Puncoviscana Formation must have been rapid and took place in a syntectonic setting (cf. Zimmermann, 2005; Keppie and Bahlburgh, 1999) spatially associated with coeval arc-like magmatism and hence unlikely represented a passive margin setting as advocated by Adams et al. (2008, 2010) and Schwartz et al. (2008).

The age distribution of detrital zircon population measured by us in the lower part of the Puncoviscana Formation shows major prominent peaks corresponding to the late Ediacaran (0.56–0.61 Ga) and late Mesoproterozoic (~1.03 Ga) and numerous subsidiary peaks between 0.6 and 1.0 and 1.1 and 2.7 Ga (Fig. 6c). The detrital zircon population published by Hausser et al. (2011) covers the same age distribution patterns, but with a strong peak at ca. 564 Ma. Similar patterns are also present in most samples analyzed by Adams et al. (2010). In general, the age distributions show an excellent match with the various provinces of the Amazon craton (Fig. 1), a link made by all workers. The prominent late Mesoproterozoic and subsidiary peaks ranging between 0.9 and 1.1 Ga representing the Sunsas belt along the southwestern margin of Amazonia. However, the generally much stronger late Ediacaran peaks are most significant, because of the evidence for Early Cambrian arc magmatism in the parts of the Puncoviscana Formation investigated by us. The Early Cambrian arc may thus be a continuation of arc magmatism that started during the Late Ediacaran along the proto-Andean margin of West Gondwana as noted by other workers (Llambías et al., 2003; Schwartz et al., 2008; Chew et al., 2008).

8. Tectonic setting of the Puncoviscana tract

The presence of small volumes of Early Cambrian (535–540 Ma) felsic and mafic arc volcanic rocks in the older parts of the Puncoviscana Formation, the arc-like composition of the associated turbidites as well the age distribution of the detrital zircons with prominent peaks lying between 569 and 523 Ma, suggests deposition adjacent to an approximately coeval arc terrane. The remnants of such an arc terrane are not exposed or preserved at the latitude of northern Argentina, but have been identified in correlatives rocks in the Pampean belt further to the south (Escayola et al., 2007; Llambías et al., 2003; Schwartz et al., 2008) where they are known as the Pampean arc (Kraemer et al., 1995; Rapela et al., 1998). Chew et al. (2008) also argued on basis of their studies that such an arc existed at the latitude of Peru. There is no evidence from regional detrital zircon studies (e.g. Adams et al., 2008, 2010) that the Puncoviscana Formation contains rocks older than the Late Ediacaran and nearly all analyzed rocks are dominated by late Ediacaran–Early Cambrian zircon populations. Hence, suggesting that deposition of all of the Puncoviscana Formation was syntectonic and coeval with arc magmatism nearby.

There is an apparent overlap in time between deformation, plutonism and deposition of turbidites in the Puncoviscana tract, with deposition apparently becoming younger from northeast to southwest. Based on these constraints, we interpret the older parts of the Puncoviscana Formation (>530 Ma), which contains the thin layers of volcanic (predominantly pyroclastic) rocks, to have been deposited in either a forearc basin or a slope basin formed on the associated accretionary wedge (Fig. 9) associated with a west-facing Pampean arc built upon the proto-Andean margin of West Gondwana (Figs. 9, 10). The dynamics of the depositional systems in forearc basins are commonly complex and may include carbonate buildups, such as locally preserved in the Puncoviscana tract, around structural highs at appropriate latitudes (Dickinson and Seely, 1979). Deposition of the younger parts (≤530 Ma) of the Puncoviscana Formation (Adams et al., 2008, 2010; Hausser et al., 2011) overlaps with Pampean–Tilcarian deformation and plutonism both in the Puncoviscana tract and Antofalla terrane of the Arequipa-Antofalla block further to the west. This part of the Puncoviscana Formation is mainly interpreted as trench and/or foreland basin deposits, which were progressively assembled into an accretionary complex as a result of foreland-propagating deformation (Fig. 9). Deposition in a foredeep setting is consistent with the paleocurrent data of Jezek et al. (1985), which showed that sediment transport was predominantly from the east or southeast, where we propose the arc-forearc block was situated The lithological resemblance between the sediments of the Puncoviscana Formation throughout this unit, regardless whether they are thought to have been

Table 6
Summary of shrimp U–Pb data from sample VLE07-04.

Spot name	ppm U	ppm Th	ppm Rad 206	$^{232}Th/^{238}U$	% err	Total $^{206}Pb/^{238}U$	% Err	Total $^{208}Pb/^{232}Th$	% Err	204corr $^{206}Pb/^{238}U$ Age	1 err	207corr $^{206}Pb/^{238}U$ Age
9582-1.1	160	143	13.6	0.92	0.39	0.099	1.4	0.0311	3.6	607	8	607
9582-2.1	124	57	17.6	0.48	0.57	0.165	1.2	0.0668	3.5	980	11	961
9582-4.1	232	55	25.8	0.25	0.58	0.130	1.4	0.0505	4.0	786	10	784
9582-8.1	218	90	70.0	0.43	0.73	0.375	1.1	0.1146	2.3	2051	19	2045
9582-9.1	443	242	39.1	0.57	0.27	0.103	1.1	0.0317	2.5	631	7	630
9582-10.1	61	60	5.0	1.02	0.57	0.097	1.6	0.0342	4.8	591	9	590
9582-10.2	203	32	16.7	0.16	0.75	0.096	1.3	0.0303	6.5	591	8	590
9582-11.1	125	187	34.7	1.54	0.31	0.322	1.2	0.0952	1.9	1799	19	1787
9582-11.2	294	79	82.5	0.28	0.50	0.327	1.1	0.0978	2.6	1825	17	1816
9582-14.1	100	48	17.7	0.50	0.63	0.207	1.3	0.0688	3.8	1209	14	1208
9582-15.1	196	165	37.9	0.87	0.34	0.225	1.1	0.0687	2.2	1307	13	1307
9582-16.1	68	38	10.1	0.57	0.68	0.174	1.4	0.0584	4.5	1030	13	1028
9582-17.1	81	32	11.9	0.41	0.76	0.171	1.4	0.0566	5.0	1019	13	1013
9582-19.1	411	219	61.2	0.55	0.29	0.174	1.1	0.0540	2.1	1032	10	1030
9582-22.1	360	172	40.3	0.49	0.32	0.130	1.1	0.0407	2.6	789	8	789
9582-28.1	142	101	10.2	0.73	0.43	0.083	1.3	0.0301	3.9	515	7	513
9582-30.1	78	18	11.1	0.23	1.01	0.167	1.4	0.0559	6.6	993	13	994
9582-31.1	127	38	18.3	0.31	0.67	0.168	1.2	0.0589	8.2	998	12	993
9582-33.1	43	26	6.4	0.63	0.84	0.174	1.6	0.0510	5.9	1033	16	1032
9582-38.1	227	180	16.3	0.82	0.32	0.084	1.2	0.0270	3.1	518	6	516
9582-40.1	186	127	32.0	0.70	0.39	0.201	1.2	0.0621	2.6	1177	13	1177
9582-44.1	240	69	35.5	0.30	0.51	0.172	1.1	0.0520	3.5	1023	11	1024
9582-45.1	73	47	11.1	0.66	0.60	0.176	1.4	0.0558	4.0	1042	13	1043
9582-46.1	148	86	10.6	0.60	0.45	0.084	1.3	0.0276	4.2	517	7	521
9582-48.1	30	23	2.7	0.78	0.90	0.106	2.0	0.0379	7.1	642	15	642
9582-49.1	241	135	18.2	0.58	0.49	0.088	1.2	0.0287	3.2	543	6	542
9582-50.1	42	3	6.3	0.08	2.21	0.177	1.6	0.0919	11.2	1041	15	1043
9582-51.1	162	114	11.7	0.73	0.40	0.085	1.3	0.0273	3.8	521	7	523
9582-51.2	255	122	18.0	0.50	0.37	0.082	1.2	0.0259	3.5	509	6	507
9582-53.1	63	30	9.1	0.48	0.74	0.168	1.4	0.0598	4.8	995	13	997
9582-53.2	255	68	36.8	0.28	0.52	0.169	1.1	0.0556	3.5	1004	11	1001
9582-54.1	511	510	148.8	1.03	0.19	0.339	1.1	0.1028	1.4	1883	17	1880
9582-54.2	443	16	40.4	0.04	1.02	0.106	1.1	0.0420	7.6	650	7	650
9582-56.1	245	137	18.2	0.58	0.34	0.086	1.2	0.0275	6.3	534	6	533
9582-57.1	119	213	10.0	1.86	0.30	0.098	1.3	0.0310	2.8	604	8	604
9582-58.1	41	19	5.9	0.47	0.89	0.168	1.5	0.0575	5.7	991	14	991
9582-59.1	216	111	32.2	0.53	0.55	0.174	1.1	0.0584	3.5	1032	11	1034
9582-61.1	201	69	25.2	0.35	0.47	0.146	1.1	0.0464	3.5	878	10	878
9582-61.2	200	75	26.5	0.38	0.49	0.154	1.8	0.0457	3.9	922	16	926
9582-64.1	189	75	25.2	0.41	0.45	0.155	1.1	0.0489	3.2	930	10	929
9582-65.1	292	224	23.1	0.79	0.28	0.092	1.1	0.0307	2.6	568	6	567
9582-65.2	256	116	20.2	0.47	0.37	0.092	1.2	0.0305	3.4	567	6	569
9582-66.1	110	74	7.9	0.70	0.47	0.084	1.4	0.0319	5.5	520	7	521
9582-67.1	91	44	8.0	0.50	0.61	0.103	1.4	0.0336	5.2	632	9	629
9582-68.1	134	70	19.7	0.54	0.48	0.172	1.2	0.0560	3.3	1022	11	1021
9582-69.1	113	80	8.2	0.73	0.44	0.085	1.3	0.0287	4.1	522	7	521
9582-70.1	51	26	3.7	0.52	0.79	0.086	1.7	0.0340	6.8	525	9	526
9582-71.1	184	137	13.2	0.77	0.36	0.084	1.2	0.0274	3.4	519	6	519
9582-73.1	455	101	105.2	0.23	0.39	0.269	1.1	0.0808	2.3	1535	14	1536
9582-74.1	113	36	23.4	0.33	0.67	0.241	1.2	0.0761	3.9	1390	15	1386
9582-76.1	94	42	19.5	0.46	0.64	0.242	1.2	0.0776	3.6	1395	16	1392
9582-78.1	157	81	40.1	0.54	0.45	0.298	1.1	0.0933	2.5	1680	17	1679
9582-80.1	190	73	26.4	0.39	0.46	0.161	1.1	0.0498	3.3	964	10	962

Errors are 1 unless otherwise specified.

deposited in the arc-trench gap or a foreland basin setting is not unexpected. For example, the forearc block exposed on the island of Timor started to supply sediments to the adjacent marine foredeep (foreland) basin after it was uplifted following the onset (ca. 4 Ma) of the Banda arc-Australia collision (Audley-Charles and Harris, 1990). Ramos (2008) proposed a similar setting for this part of the tectonic evolution and is also consistent with the interpretations of Keppie and Bahlburgh (1999) and Zimmermann (2005). Whether the proposed foredeep setting was a trench or a foreland basin depends on whether the syn-to post-tectonic calc-alkaline magmatism, such as represented by the Tastil and Cañani plutons, formed part of an arc, was syn-collisional and hence, presumably related to slab breakoff, or a combination of both. In the former model, the Puncoviscana tract records arc-trench migration (Fig. 9); the latter two options, which we favour (see below) imply that a continental margin (Arequipa-Antofalla block) had entered the trench and hence, the trench had become a foreland basin (e.g. Dickinson, 1977). An accretionary complex setting is supported by the style of deformation and metamorphism (see above and Do Campo and Nieto, 2003). In general, the rocks and structures of the Puncoviscana tract resemble those present in parts of Southern Uplands tract in southern Scotland and central Ireland, which is generally interpreted as a Late Ordovician-Early Silurian accretionary complex (Legget et al., 1982; Van Staal et al., 1998) and/or a foreland-propagating fold-thrust belt (Stone et al., 1987).

Table 7
Summary of U-Pb TIMS analyses of zircons samples VLE07-104 and VLE07-113.

Fraction	Wt. μg	U ppm	Pb ppm	$^{206}Pb/^{204}Pb$	Pb pg	$^{208}Pb/^{206}Pb$	$^{207}Pb/^{235}U$	1SE Abs
VLE-07-104								
A2 (Z)	4	166.85	14.94	1766.7	2	0.14	0.69866	0.00116
A3 (Z)	4	163.74	14.8	1519.6	2	0.15	0.69841	0.00117
VLE-07-113								
A1 (Z)	14	152.09	13.94	9950.4	0	0.2	0.67782	0.00084
A3 (Z)	7	154.88	14.51	4155	1	0.22	0.68307	0.00093

	$^{206}Pb/^{238}U$	1SE Abs	Correlation coefficient	$^{207}Pb/^{206}Pb$	1SE Abs	$^{206}Pb/^{238}U$ Age(Ma)	2SE	$^{207}Pb/^{235}U$ Age (Ma)
VLE-07-104								
A2 (Z)	0.08691	0.00009	0.779452248	0.0583	0.00006	537.2	1.1	538
A3 (Z)	0.08686	0.00008	0.788481197	0.05832	0.00006	537	1	537.8
VLE-07-113								
A1 (Z)	0.08475	0.00008	0.897327043	0.058	0.00003	524.4	1	525.5
A3 (Z)	0.08504	0.00009	0.872059643	0.05825	0.00004	526.2	1	528.6

	$^{207}Pb/^{235}U$ age (Ma)	2SE	$^{207}Pb/^{206}Pb$ age (Ma)	2SE	Discord (%)
VLE-07-104					
A2 (Z)	538	1.4	541.2	4.6	0.77
A3 (Z)	537.8	1.4	541.6	4.8	0.9
VLE-07-113					
A1 (Z)	525.5	1	529.9	2.5	1.08
A3 (Z)	528.6	1.1	539.3	3	2.54

9. Arequipa-Antofalla terranes: a ribbon-like crustal block

Our analyses of the inherited zircons in the Cerro Negro orthogneiss in the southern domain of the Antofalla terrane gave ages of 654 Ma, 875 Ma, 940 Ma, 1040 Ma, 1175 Ma, 1392 Ma, 1500 Ma, 1681 Ma and 1881 Ma, which are similar to the ages described for the northern and central domains of the Arequipa-Antofalla block by Loewy et al. (2004) and previous data summarized therein. Hence, we follow earlier interpretations (e.g. Rapela et al., 2007) that consider all three domains of the Arequipa-Antofalla terrane part of one crustal block by the end of the Mesoproterozoic, with no evidence of a separation into isolated terranes during Ediacaran–Early Cambrian as proposed by Ramos (2008).

10. Implications of Pb-isotope data for extent and involvement of the Arequipa-Antofalla block in the Tilcarian–Pampean orogenic cycle

Pb–Pb isotopic analyses of the K-feldspars of the Cañani pluton yielded high $^{207}Pb/^{204}Pb$ ratios of 15.714–15.746 and $^{206}Pb/^{204}Pb$ ratios of 18.248–18.266 and high $^{207}Pb/^{204}Pb$ ratios (relative to $^{206}Pb/^{204}Pb$), which plot above Stacey and Kramers (1975) crustal evolution curve (Fig. 7f). These ratios are similar to those measured in basement rocks of the northern domain of the Arequipa-Antofalla block, and are slightly less radiogenic than the peraluminous granites that intruded the eastern Pampean Ranges further south. The latter have Pb-isotope ratios ($^{206}Pb/^{204}Pb$ versus $^{207}Pb/^{204}Pb$) similar to those measured in the Mesoproterozoic

Table 8
Summary of Pb–Pb LA-ICPMS-MC analyses of feldspars sample VLE07-113.

Sample	$^{208}Pb/^{204}Pb$	$^{207}Pb/^{204}Pb$	$^{206}Pb/^{204}Pb$	$^{208}Pb/^{206}Pb$	$^{208}Pb/^{207}Pb$	$^{207}Pb/^{206}Pb$	$^{205}Pb/^{203}Pb$	f
VLE07-113-1								
Average	38.262	15.746	18.286	2.0924	2.4299	0.8611	2.3889	−1.187
SD	2.832	1.166	1.353	0.0111	0.0093	0.0050	0.0000	0.517
SE	0.241	0.099	0.115	0.0009	0.0008	0.0004	0.0000	0.044
Count	138	138	138	138	138	138	138	138
Time (s)	28	28	28	28	28	28	28	28
VLE07-113-2								
Average	38.1750	15.7140	18.2480	2.0921	2.4293	0.8612	2.3889	−1.2051
SD	3.2175	1.3180	1.5473	0.0109	0.0103	0.0054	0.0000	0.4472
SE	0.2822	0.1156	0.1357	0.0010	0.0009	0.0005	0.0000	0.0392
Count	130	130	130	130	130	130	130	130
Time (s)	26	26	26	26	26	26	26	26
VLE07-113-3								
Average	38.2617	15.7463	18.2859	2.0924	2.4299	0.8611	2.3889	−1.1874
SD	2.8322	1.1656	1.3530	0.0111	0.0093	0.0050	0.0000	0.5167
SE	0.2411	0.0992	0.1152	0.0009	0.0008	0.0004	0.0000	0.0440
Count	138	138	138	138	138	138	138	138
Time (s)	27.6	27.6	27.6	27.6	27.6	27.6	27.6	27.6
VLE07-113-4								
Average	38.185	15.717	18.251	2.0924	2.4295	0.8613	2.3889	−1.191
SD	3.215	1.317	1.546	0.0114	0.0105	0.0054	0.0000	0.481
SE	0.282	0.116	0.136	0.0010	0.0009	0.0005	0.0000	0.042
Count	130	130	130	130	130	130	130	130
Time (s)	26	26	26	26	26	26	26	26

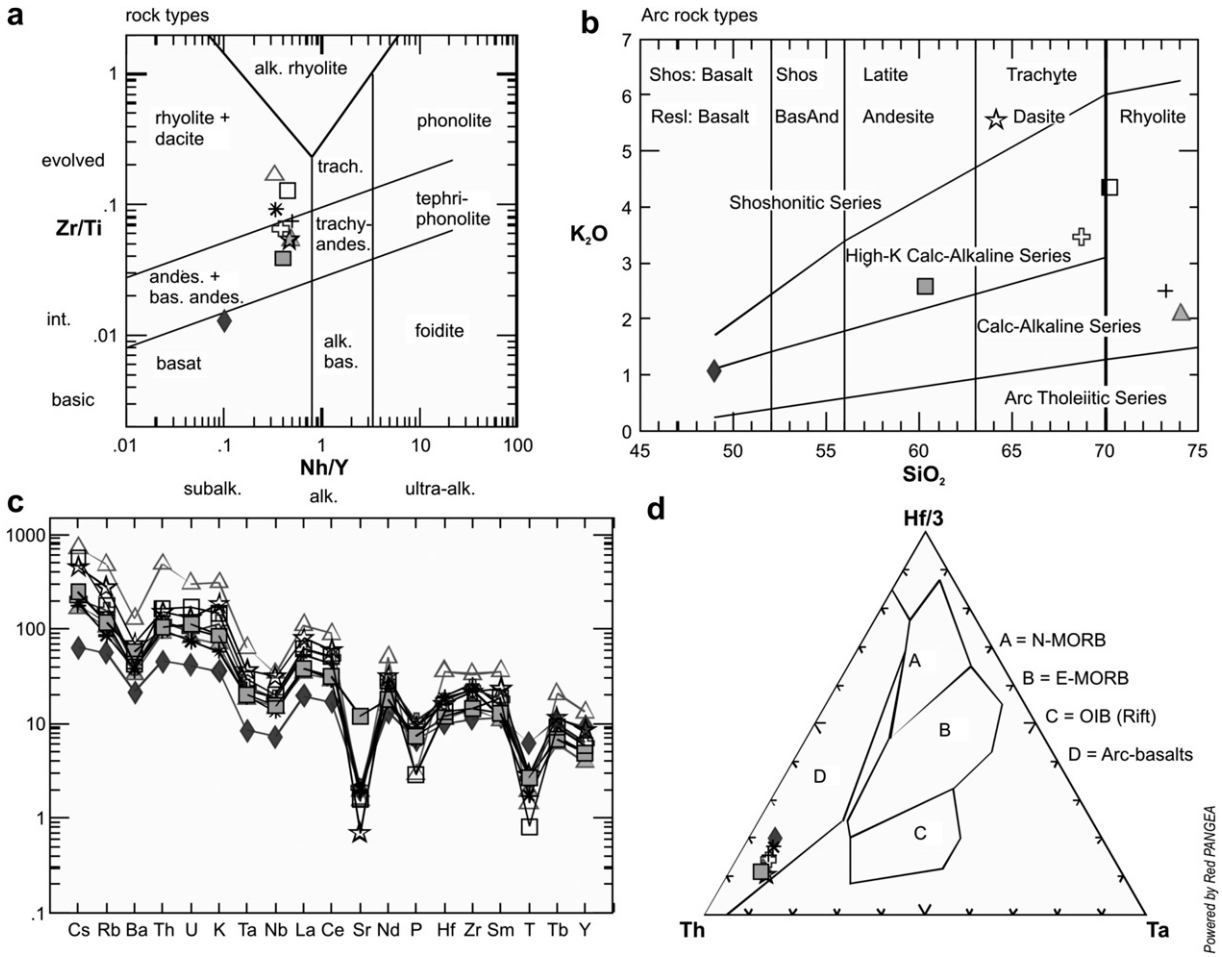

Fig. 8. (a) Plot of the tuff beds and andesitic–basaltic volcanic and volcaniclastic rocks of the Puncoviscana Formation, Cañani quartz diorite and Cerro Negro (Antofalla) ortogneiss in the Zr/Ti vs Nb/Y discrimination diagram of Winchester and Floyd (1977); (b) same in SiO_2 vs K_2O classification diagram of Pecerillo and Taylor (1976); (c) same in primordial mantle normalized spider diagrams (Wood et al., 1979); (d) same in tectonic setting discrimination diagram of Wood (1980). All rocks plot in field of arc volcanic rocks.

basement rocks of the central domain of the Arequipa-Antofalla block (Schwartz and Gromet, 2004). The Pb-isotope data thus suggests that the exotic basement block postulated to be situated beneath the western part of the Eastern Pampean ranges (Escayola et al., 2007) may be a southern extension of the Arequipa-Antofalla crustal block. Support for such a correlation is also provided by the 529–520 Ma zircon ages of syn-collision granites and tonalites in the Eastern Pampean Ranges, which are coeval with the Cerro Negro orthogneiss and the Canañí and Tastil plutons described in this study. The ridge-subduction model of Schwartz et al. (2008) is inconsistent with generation of these plutons in the Arequipa-Antofalla crustal block. We therefore propose that the western half of the Pampia terrane of Ramos et al. (2010) is underlain by the Arequipa-Antofalla crustal block (Fig. 9).

11. Discussion and tectonic model

During the Late Ediacaran–Early Cambrian (>530 Ma) the Puncoviscana Formation is interpreted to have been deposited mainly in the arc-trench gap associated with a west-facing Pampean arc and subsequently (≤530 Ma) mainly in a syn-collisional (Pampean–Tilcarian orogeny) foreland basin, formed as a result of underthrusting of the Arequipa-Antofalla block beneath the Pampean arc (Fig. 9). Such a tectonic model (Figs. 9, 10) is similar to the Ediacaran–Early Cambrian evolution proposed for the proto-Andean margin of western Gondwana in the Pampean ranges by Rapela et al. (1998), Escayola et al. (2007), and to the north at the latitude of Peru by (Chew et al., 2008). Together with the work by Schwartz et al. (2008), these workers provided independent evidence for the presence of an extensive west-facing Ediacaran to Early Cambrian Pampean arc along the length of the proto-Andean margin (Fig. 3). A remaining question is when the Pampean arc was initiated. The detrital zircons in the Puncoviscana Formation suggest this arc existed by at least ca. 570 Ma, which is also implied by the data of Escayola et al. (2007) who explained formation of this arc as a result of a subduction polarity reversal induced by accretion of the 640–620 Ma Córdoba arc-backarc system to the Río de la Plata craton (Fig. 10). Accretion of the Córdoba arc-backarc system was probably related to closure of the Goiás Ocean (approximately along the Transbrasiliano lineament in Fig. 10) and amalgamation of Amazonia to West Gondwana (e.g. Pimentel et al., 2000; Cordani et al., 2009; Cordani et al., 2010). The Córdoba arc-backarc system accretion to the Río de la Plata craton would represent the last phase of the closure of the Neoproterozoic Goiás Ocean, which started around 900 Ma in the northeaster sector of the Transbrasiliano lineament with formation of the juvenile Goiás magmatic arc. The Goias arc was caught-up in the main Brasiliano collisional event (650–580 Ma), which amalgamated the various continental cratons into West Gondwana (Fig. 10) (Pimentel et al., 2000, 2011; Cordani et al., 2010; Della Giustina

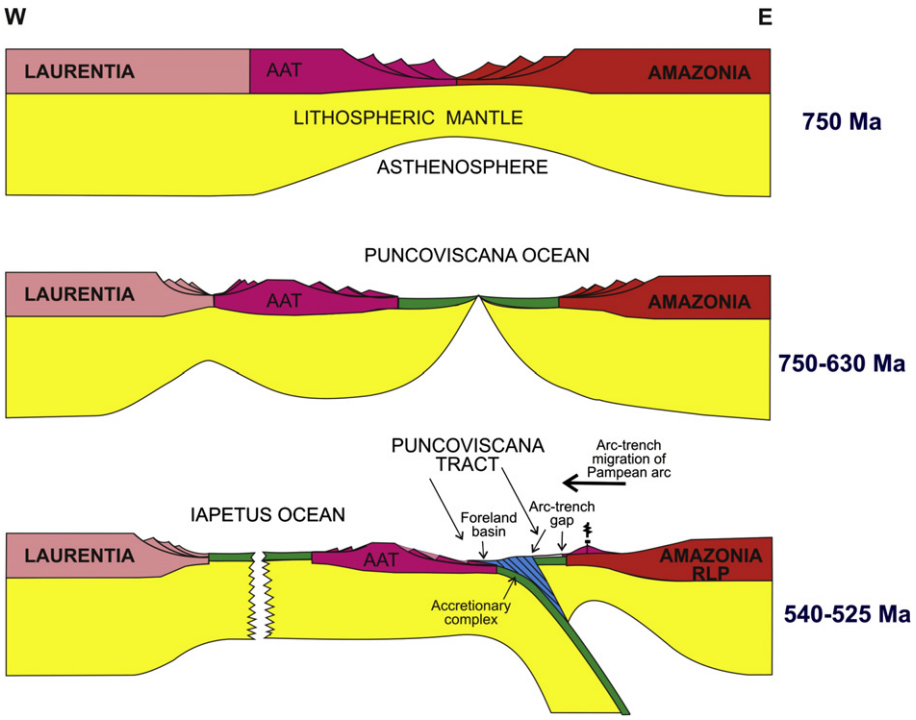

Fig. 9. Tectonic model of the Late Neoproterozoic-Early Cambrian evolution of Rodinia break-up in the Laurentia-Amazonia sector. We propose that first Amazonia rifted-off, approximately along the Grenville-age suture with the Arequipa-Antofalla block prior to 650 Ma, opening the Puncoviscana Ocean. After the Ediacaran accretion of south-western Amazonia to Gondwana (Fig. 8) as a result of the final closure of the Neoproterozoic Goiás Ocean, a new east-dipping subduction zone was initiated along the proto-Andean margin of West Gondwana, which was accompanied by and/or led to rifting-off of the Arequipa-Antofalla block from Laurentia, probably also near its old suture between 600 and 570 Ma, opening the Iapetus Ocean in its wake.

et al., 2011). The presence of significant Grenville-age inheritance (Escayola et al., 2007) suggests the Córdoba arc-backarc system may have been built upon a promontory-like extension of the Amazonian Sunsas belt to the south, which was also suggested by Cordani et al. (2010) (if correct this extension corresponds to the eastern part of the Pampia terrane of Ramos et al., 2010). Zircon populations with ages coeval to the Córdoba arc commonly show up as separate peaks in the Puncoviscana tract (e.g. Adams et al., 2008, 2010). Construction of a new west-facing arc during the Ediacaran is also consistent with the U–Pb zircon ages of ca. 584 Ma and ca. 555 Ma for silicic calc-alkaline volcanic rocks of the Eastern Pampean ranges given by Llambías et al. (2003) and Schwartz et al. (2008) respectively. The Pampean arc was situated inboard of the Arequipa-Antofalla block, hence the latter had to be separated from West Gondwana by an oceanic seaway. We refer to this seaway as the Puncoviscana Ocean following earlier workers (Rapela et al., 1998), which according to our data and that of Chew et al. (2007, 2008) extended north along the proto-Andean margin into Bolivia and Peru (Fig. 10).

Evidence for involvement of the Arequipa-Antofalla block (lower plate) in the Pampean–Tilcarian collision (cf. Loewy et al., 2004) at present is sparce (e.g. Casquet et al., 2008), although it is supported by the Pb isotopic data of the Canañí pluton and the U–Pb zircon provenance of the Cerro Negro orthogneiss presented herein in addition to other data discussed earlier in Section 2.4. Regardless, relatively soft collisions, such as the Tilcarian–Pampean orogeny is considered, rarely extend far into the foreland. Parts of the Taconic orogeny in the northern Appalachians of Canada show similar features. Only locally a narrow belt of metamorphic tectonites was developed here in rocks of the downgoing Laurentian plate (Van Staal et al., 2009).

The Arequipa-Antofalla block is generally inferred to has been accreted originally to the Amazonian Sunsas Belt during Grenvillian time (Loewy et al., 2004; Chew et al., 2007, 2008) and subsequently as part of greater Amazonia, to Laurentia during assembly of Rodinia (Ramos, 2008). Pb isotopic data suggest that remnants of such greater Amazonia are present in basement rocks of the southern and central Appalachians (Loewy et al., 2003), which thus may represent remnants of the Arequipa-Antofalla block left behind when it rifted-off Laurentia. Hence, a subsequent separation of the Arequipa-Antofalla crustal block from Amazonia probably took place during the Neoproterozoic. Loewy et al. (2004) related an Ediacaran-Cryogenian dacite dike of ca. 635 Ma in the Arequipa-Antofalla block to rifting and break-up of Rodinia. In addition, Casquet et al. (2008) presented late Ediacaran ages (ca. 570 Ma) for rifting-related syenite and carbonatite in the Sierra de Maz in Argentina, which is considered to form part of the Arequipa-Antofalla block by the authors and us. Inherited zircons with ages of ca. 875–654 Ma in the Cerro Negro orthogneiss investigated by us (see above), probably also reflect magmatism related to Rodinia rifting and break-up. Such ages with a main peak at 777 Ma also are prominent in the detrital zircon populations of the Puncoviscana Formation (Fig. 6c), suggesting such magmatism should exist in western Amazonia. An important question is whether the Arequipa-Antofalla block was still partly attached or not to Laurentia when it separated from Amazonia to form the Puncoviscana Ocean. If it was already separated from Laurentia, the Iapetus Ocean had probably opened earlier during the Cryogenian. If not, the Iapetus Ocean opened later, when the Arequipa-Antofalla block departed from Laurentia (e.g. Cordani et al., 2009, p. 405). We favour the latter option, because it is most consistent with existing data. In this context, it is significant to mention that the Early Cambrian rift-drift transition, which is nearly coeval along the whole length of the Appalachian margin of Laurentia (Bond et al., 1984; Hibbard et al., 2007), is unlikely related to opening of the Iapetus Ocean, but rather relates to subsequent departure of crustal

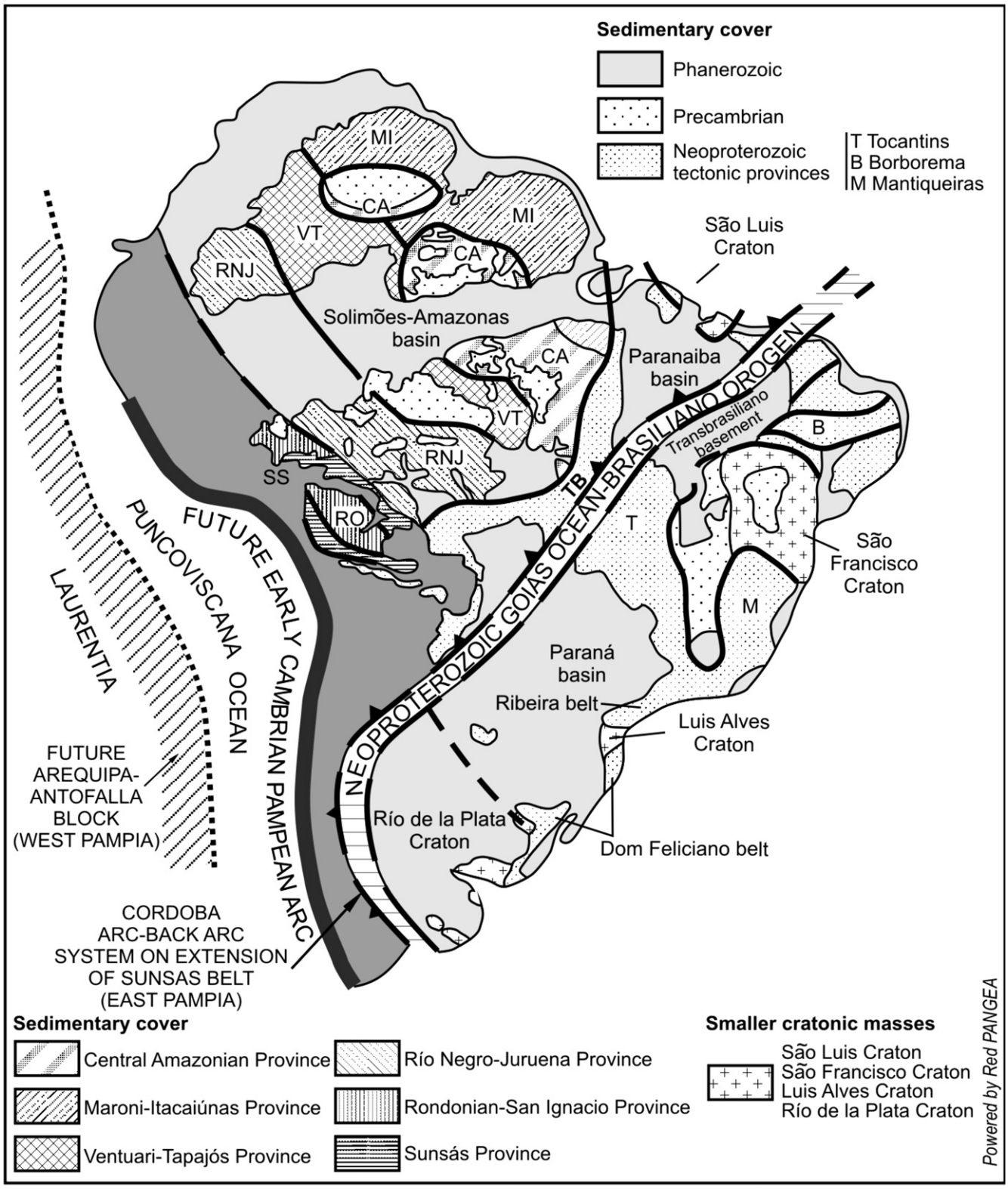

Fig. 10. Diachronous closure of the Goiás Ocean starting at the northeastern end of the Transbrasiliano Lineament and progressively closing to the south amalgamating the Amazonian and the Rio de La Plata cratons. The 640–620 Ma Cordoba arc – back-arc system of Escayola et al. (2007) is inferred to have formed on a promontory of Amazonia mainly underlain by the Sunsas belt. This collision led to initiation of east-directed subduction in the Puncoviscana Ocean and construction of the Pampean arc on the proto-Andean margin of West Gondwana shown in Fig. 1.

ribbons such as the Dashwoods block in the northern Appalachians (Waldron and van Staal, 2001; Cawood et al., 2001; Allen et al., 2010) and the Precordillera/Cuyania block in the southern Appalachians (Thomas and Astini, 1996). Multistage rifting and an Ediacaran opening of the Iapetus Ocean are also most consistent with paleomagnetic constraints (McCausland et al., 2007) and the presence of distinct pulses of rift-related magmatism. Iapetus probably opened during or shortly after the main pulse between

615 and 580 Ma (Cawood et al., 2001; Waldron and van Staal, 2001). The future Appalachian margin of Laurentia was at this time situated inboard of the ribbon blocks that rifted-off during the Early Cambrian. Hence, the evidence for this event is either poorly known or not preserved in the late Ediacaran sedimentary record of the Appalachian margin of Laurentia.

Our interpretations imply that Ediacaran–Early Cambrian closure of the Pucoviscana Ocean was coeval with and tectonically related to the opening of Iapetus. Slab-pull forces acting on the downgoing plate may have contributed to rifting of the Arequipa-Antofalla block from Laurentia. In addition, our model demands that the trailing margin of the Arequipa-Antofalla block while converging with West Gondwana as a result of the closure of the Puncoviscana Ocean became the basement to the conjugate passive margin of Iapetus. However, formation of the Famatinian arc-forearc system on the Arequipa-Antofalla block (Bahlburg and Hervé, 1997; Rapela et al., 1998; Ramos, 2008) shortly after closure of the Puncoviscana Ocean, between 505 and 455 Ma, probably obscured and/or destroyed most evidence of such a margin, which in any case must have been relatively short-lived.

The ages of the syn-to post-tectonic Early Cambrian intrusions in the Puncoviscana Formation, such as the Cañani and Tastil plutons, overlap with the age of the Cerro Negro orthogneiss in the southern domain of the Arequipa-Antofalla block and syn-collision plutons dated in the eastern Pampean ranges (Escayola et al., 2007). These Tilcarian plutons suggest that the collision between the Arequipa-Antofalla block and West Gondwana had started by circa 530 Ma (Fig. 9). The 540–535 Ma calc-alkaline volcanism identified by us in the Puncoviscana Formation should thus record the last gasps of Pampean arc volcanism. The demise of the Pampean–Tilcarian collision and its possible collapse are at present poorly constrained. The interpretations of Hongn et al. (2010) suggest that a phase of orogenic collapse started near the end of the Early Cambrian, which at least in part, was responsible for deposition of the Meson Group.

Following the Pampean collision, the east-dipping subduction zone stepped-outboard of the accreted Arequipa-Antofalla block by Middle–Late Cambrian times (505–500 Ma) and initiated the Famatinian orogenic cycle (Ramos, 1986, 1988; Pankhurst and Rapela, 1998; Quenardelle and Ramos, 1999) further to the west.

Acknowledgements

We are grateful to Ricardo Omarini of Salta University for discussions and companionship in the field during several field-trips. CONICET-IDEAN (Instituto de Estudios Andinos, Universidad de Buenos Aires) and the Geological Survey of Canada under TGI 3, financially and logistically supported this project. The unfailing financial support from Neil Rogers in his role as leader of Appalachian TGI 3 at the GSC in Ottawa was instrumental in carrying out this project. His recognition of the significance of this research for van Staal's ongoing studies related to opening of Iapetus and the Appalachian orogen, showed considerable intellectual depth. This paper benefited from the editing by Alex Zagorevski the comments of three anonymous reviewers and Dr. Victor Ramos, regional editor of JSAES. We also appreciate the help of Mario Campaña from Red Pangea for making some of the figures in great haste. This is Geological Survey of Canada publication 20110098.

References

Aceñolaza, F.G., Toselli, F.R., 1981. Geología del noroeste Argentino: San Miguel de Tucumán, Facultad de Ciencias Naturales, Universidad Nacional de Tucumán, 212 p.

Aceñolaza, F.G., Toselli, A.J., 1976. Consideraciones estratigráficas y tectónicas sobre el Paleozoico inferior del noroeste argentino. II Congreso Latino-Americano de Geología Venezuela T. 2, 741–754.

Aceñolaza, F.G., Miller, H., 1982. Early Paleozoic orogeny in southern South America. Precambrian Research 17, 133–146.

Aceñolaza, F.G., Miller, H., Toselli, A.J., 1988. The Puncoviscana Formation (late Precambrian-Early Cambrian). Sedimentology, tectonometamorphic history and age of the oldest rocks of NW Argetina. In: BahlburgH., BreitkreuzC., GieseP (Eds.), The Southern Central Andes: Contributions to Structure and Evolution of and Active Continental Margin. Lecturer Notes on Earth Sciences, 17. Springer Verlag, Berlin, pp. 25–38.

Adams, C., Miller, H., Toselli, A.J., 2008. Detrital zircon U–Pb ages of the Puncoviscana Formation, Late Neoproterozoic – Early Cambrian, of NW Argentina: provenance area and maximum age of deposition. In: Linares, E., Cabaleri, N.G., Do Campo, M.D., Duchos, E.I., Panarello, H.O. (Eds.), (VI SSAGI) VI South American Symposium on Isotope Geology. Compilers Proceedings. Trabajo CD Room, 4 pp.

Adams, C.J., Miller, H., Aceñolaza, F.G., Toselli, A.J., Griffin, W.L., 2010. The Pacific Gondwana margin in the late Neoproterozoic – early Paleozoic: detrital zircon U–Pb ages from metasediments in northwest Argentina reveal their maximum age, provenance and tectonic setting. Gondwana Research, 698. doi:10.1016/j.gr.2010.05.002.

Allen, J.S., Thomas, W.A., Lavoie, D., 2010. The Laurentian margin of northeastern North America. In: Tollo, R.P., Batholomew, M.J., Hibbard, J.P., Karabinos, P.M. (Eds.), From Rodinia to Pangea: The lithotectonic record of the Appalachian region. Geological Society of America Memoir 206, pp. 71–90.

Allmendinger, R., Jordan, T., Palma, M., Ramos, V.A., 1982. Perfil structural de la Puna Catamarqueña (25–27°), Argentina. 5° Congreso Latinoamericano de Geologia, Actas, Buenos Aires 1, 499–518.

Audley-Charles, M.G., Harris, R.A., 1990. Allochthonous terranes of the Southwest Pacific and Indonesia. Philosophical Transactions of the Royal Society of London Series A 331, 571–587.

Bahlburg, H., Hervé, F., 1997. Geodynamic evolution and tectonostratigraphic terranes of northwestern Argentina and northern Chile. Geological Society of America Bulletin 109, 869–884.

Bhathia, M.R., Crook, K.A.W., 1986. Trace elements characteristics of greywacke and tectonic setting discrimination of sedimentary basins. Contribution Mineralogy and Petrology 92, 181–193.

Becchio, R., Lucassen, F., Franz, G., Viramonte, J., Wemmer, K., 1999. El basamento paleozoico inferior del noroeste de Argentina (23°–27°S) metamosrfismo y geocronologia. In: Gonzalez Bonorino, G., Omarini, R., Viramonte, J. (Eds.), Geologia del Noroeste Argentino. XVI Congreso Geologico Argentino, Salta, vol. 1, pp. 58–72.

Bond, G.C., Nickeson, P.A., Kominz, M.A., 1984. Break-up of a supercontinent between 625 Ma and 555 Ma: new evidence and implications for continental histories. Earth and Planetary Science Letters 70, 325–345.

Cardona, A., Cordani, U.G., Ruiz, J., Valencia, V.A., Armstrong, R., Chew, D., Nutman, A., Sanchez, A.W., 2009. U-Pb zircon geochronology and Nd isotopeic signatures of the pre-Mersozoic metamorphic basement of the eastern Peruvian Andes: growth and provenance of a Late Neoproterozoic to Carboniferous Accretionary Orogen on the northwest margin of Gondwana. The journal of Geology 117, 285–305.

Casquet, C., Pankhurst, R.J., Galindo, C., Rapela, C., Fanning, C.M., Baldo, E., Dahlquist, J., Gonzales Casado, J.M., Columbo, F., 2008. A deformed alkaline igneous rock-carbonatite complex from the western Sierras Pampeanas, Argentina: evidence for late Neoproterozoic opening of the Clymene Ocean? Precambrian Research 165, 205–220.

Cawood, P.A., McCausland, P.J.A., Dunning, G.R., 2001. Opening Iapetus: constraints from the Laurentian margin in Newfoundland. Geological Society of America Bulletin 113, 443–453.

Chew, D.M., Kosler, J., Whitehouse, M.J., Gutjahr, M., Spikins, R.A., Miskovic, A., 2007. U–Pb geochronologic evidence for the evolution of the Gondwanan margin of the north-central Andes. GSA Bulletin 119 (5/6), 697–711.

Chew, D.M., Magna, T., Kirkland, C.L., Miskovic, A., Cardona, A., Spikings, R., Schaltegger, U., 2008. Detrital zircon fingerprint of the Proto-Andes: evidence for a neoproterozoic passive margin? Precambrian Research 167, 186–200.

Coira, B., Davidson, J., Mpodozis, C., Ramos, V.A., 1982. Tectonic and magmatic evolution of the Andes of northern Argentina and Chile. Earth Science Reviews 18, 303–332.

Collo, G., Astini, R., Cawood, P.A., Buchan, C., Pimentel, M., 2009. U–Pb detrital zircon ages and Sm–Nd isotopic features in low grade metasedimentary rocks of the Famatinia belt: implications for the late Neoproterozoic-early evolution.

Cordani, U.G., Teixeira, W., D'Agrella-Filho, Trindade, R.L., 2009. The position of Amazonian Craton in Supercontinents. Gondwana Research 15, 396–407.

Cordani, U.G., Teixeira, W., Tassinari, C.C.G., Coutinho, J.M.V., Ruiz, A.S., 2010. The Rio Apa Craton in Mato Grosso do Sul (Brazil) and northern Paraguay: geochronological evolution, correlations and tectonic implications for Rodinia and Gondwana. American Journal of Science 310, 981–1023.

Dalmayrac, B., Lancelot, J.R., Leyreloup, A., 1980. La chain hercynienne d' Amerique du sud, structure et evolution d' un orogene intracratonique. Geol Rundsch 69, 1–21.

Dalziel, I.W.D., 1997. Neoproterozoic–Paleozoic geography and tectonics, review hypothesis, enviromental speculations. Geological Society of America Bulletin 109, 16–42.

Davis, W.J., Gariepy, C., van Breemen, O., 1996. Pb isotopic composition of late Archean granites and the extent of recycling early Archean crust in the Slave Province, northwest Canada. Chemical Geology 130, 255–269.

Della Giustina, M.E.S., Pimentel, M.M., Ferreira-Filho, C.F., Hollanda, M.H.B.M., 2011. Dating coeval mafic magmatism and ultra-high temperature metamorphism in the Anápolis-Itauçu Complex, Central Brazil. Lithos 124, 92–102.

Dickinson, W.R., 1977. Tectono-stratigraphic evolution of subduction-controlled sedimentary assemblages. In: Talwani, M., Pitman, W.C. (Eds.), Island Arcs, Deep Sea Trenches and Back-Arc Basins. Maurice Ewing Series 1. American Geophysical Union, pp. 33–40.

Dickinson, W.R., Seely, D.R., 1979. Structure and stratigraphy of forearc regions. American Association of Petroleum Geologists Bulletin 63, 2–31.

Do Campo, M., Nieto, F., 2003. Transmission electron microscopy study of very low-grade metamorphic evolution in Neoproterozoic pelites of the Puncoviscana formation (Cordillera Oriental, NW Argentina). Clay Mineralogy 38, 459–481.

Durand, F.R., Aceñolaza, F.G., 1990. Caracteres biofaunisticos, paleoecológicos y 749 paleogeográficos de la Formación Puncoviscana (Precámbrico superior-Cámbricinferior) del Noroeste Argentino. In: Aceñolaza, F.G., Miller, H., Toselli, A.J. (Eds.), El Ciclo Pampeano en el Noroeste Argentino. Serie: Correlación Geológica, vol. 4, pp. 71–112.

Escayola, M.P., Pimentel, M.M., Armstrong, R., 2007. A Neoproterozoic Back-Arc Basin: SHRIMP U–Pb and Sm––Nd isotopic evidence from the Eastern Pampean Ranges, Argentina. Geology 35 (6), 495–498.

Evans, D.A.D., 2009. The paleomagnetically viable and long-lived and all-inclusive Rodinia supercontinent reconstruction. In: Murphy, J.B., Keppie, J.D., Hynes, A.J. (Eds.), Ancient Orogens and Modern Analogues. Geological Society London Special Publication 327, pp. 371–404.

Gariepy, C., Allegre, C.J., 1985. The lead isotope geochemistry and geochronology of late-kinematic intrusives from the Abitibi greenstone belt, and the implications for late Archean crustal evolution. Geochimica et Cosmochimica Acta 49, 2371–2383.

Hausser, N., Matteini, M., Omarini, R.H., Pimentel, M.M., 2011. Combined U–Pb and Lu–Hf isotope data on turbidites of the Paleozoic basement of NW Argentina and petrology of associated igneous rocks: implications for the tectonic evolution of western Gondwana between 560 and 460 Ma. Gondwana Research 19 (1), 100–127.

Hibbard, J.P., van Staal, C.R., Rankin, D.W., 2007. A comparative analysis of pre-Silurian building blocks of the northern and southern Appalachians. American Journal of Science 307, 23–45.

Hoffman, P.F., 1991. Did the breakout of Laurentia turn Gondwanaland inside-out? Science 252, 1409–1412.

Hongn, F.D., 1994. Estructuras Precámbricas y Paleozóicas del basamento del borde oriental de la Puna; su aplicación para el análisis regional de la Faja Eruptiva. Revista de la Asociación Geológica Argentina 49, 256–268.

Hongn, F., Tubia, J.M., Aranguren, A., Vegas, N., Mon, R., Dunning, G., 2010. Magmatism coeval with lower Paleozoic shelf basins in NW-Argentina (Tastil batholiyh): Constraints on current stratigraphic and tectonic interpretations. Journal of South American Earth Sciences 29, 289–305.

Housh, T., Bowring, S.A., 1991. Lead isotope heterogeneities within alkali feldspars: implications for the determination of initial lead isotopic compositions. Geochimica et Cosmochimica Acta 55, 2309–2316.

Jezek, P., Miller, H., 1987. Petrology and facies analysis of turbiditic sedimentary rocks of the Puncoviscana through (Upper Precambrian-Lower Cambrian) in the basement of the NW Argentine Andes. in Gondwana Six: structure, tectonics, and geophysics. Geophysical Monograph 40, 287–293.

Jezek, P., Willner, A.P., Aceñolaza, F.G., Miller, H., 1985. The Puncoviscana trough – a large basin of Late Precambrian to Early Cambrian age on the Pacific edge of the Brazilian shield. Geologische Rundschau 74 (3), 573–584.

Keppie, J., Bahlburgh, H., 1999. Puncoviscana Formation of northwestern and central Argentina: passive margin or foreland basin deposit. In: Ramos, V.A., Keppie, J.D. (Eds.), Laurentia–Gondwana Connections Before Pangea. Geological Society of America Special Paper 336, pp. 139–143.

Kley, J., 1996. Transition from basement-involved to thin -skinned thrusting in the cordillera Oriental of southern Bolivia. Tectonics 15, 763–775.

Kraemer, P.E., Escayola, M.P., Martino, R.D., 1995. Hipotesis sobre la evolucion tectonica neoproterozoica de las Sierras Pampeanas de Cordoba (30° 40′–32° 40′), Argentina. Revista de la Asociación Geológica Argentina 50, 47–59.

Llambías, E.J., Gregori, D., Basei, M.A., Varela, R., Prozzi, C., 2003. Ignimbritas riolíticas neoproterozoicas en la Sierra Norte de Córdoba evidencia de un arco magmático temprano en el ciclo Pampeano? Revista de la Asociación Geológica Argentina 58 (4), 572–582.

Legget, J.K., McKerrow, W.S., Casey, D.M., 1982. The anatomy of an accretionary forearc: the Southern Uplands of Scotland. Geological Society London Special Publication 10, 494–520.

Loewy, S.L., Connelly, J.N., Dalziel, I.W.D., Gower, C.F., 2003. Eastern Laurentia in rodinia: constraints from whole-rock Pb and U/Pb geochronology. Tectonophysics 375, 169–197.

Loewy, S.L., Connelly, J.N., Dalziel, I.W.D., 2004. An orphaned basement block: The Arequipa-Antofalla Basement of the central Andean margin of South America. GSA Bulletin 116 (1, 2), 171–187.

Ludwig, K.R., 2003. User's Manual for Isoplot/Ex rev.3.00: A Geochronological Toolkit for Microsft Excel. In: Special Publication, 4. Berkeley Geochronology Center, Berkeley, California, U.S.A.

Manhes, G., Allègre, C.J., Dupré, B., Hamelin, B., 1980. Lead isotope study of basic-ultrabasic layered complexes: Speculations about the "age of the Earth" and primitive mantle characteristics. Earth and Planetary Science Letters 47, 370–380.

McCausland, P.J.A., van der Voo, R., Hall, C.M., 2007. Circum-Iapetus paleogeography of the Precambrian-Cambrian transition with a new paleomagnetic constraint from Laurentia. Precambrian Research 156, 125–152.

Matteini, M., Hauser, N., Pimentel, M.M., Omarini, R., Dantas, E.L., Buhn, B.M., 2008. Combined in situ U–Pb, Lu–Hf and Sm–Nd systematics applied to the Tastil batholith, Eastern Cordillera, NW Argentina: implications for the evolution of Western margin of Gondwana during the Early Paleozoic. VI South American Symposium on Isotope Geology, 4 pp. CD-ROM.

Monger, J.H.W., Price, R.A., Tempelman-Kluit, D.J., 1982. Tectonic accretion and the origin of two major metamorphic and plutonic welts in the Canadian Cordillera. Geology 10, 70–75.

Omarini, R.H., Sureda, R., Toselli, A.J., Rossi, J.N., 1999. Magmatismo. En: Geología del Noroeste Argentino. In: González Bonorino, G., Omarini, R., Viramonte, J. (Eds.), Relatorio del XIV Congreso Geológico Argentino. Tomo I, pp. 29–40.

Pankhurst, R.J., Rapela, C.W., 1998. The proto-Andean margin of Gondwana: an introduction. Geological Society of London Special Publications 142, 1–10.

Parrish, R.R., Roddick, J.C., Loveridge, W.D., Sullivan, R.W., 1987. Uranium-lead analytical techniques at the Geochronology Laboratory, Geological Survey of Canada: In: Radiogenic age and isotope studies, Report 1: Geological Survey Canada Paper 87–2, 3–7.

Pecerillo, A., Taylor, S.R., 1976. Geochemistry of Eocene calc-alkaline volcanic rocks from the Kastamonu area, Northern Turkey. Contributions to Mineralogy and Petrology 58, 189–202.

Pimentel, M.M., Fuck, R.A., Jost, H., Ferreira Filho, C.F., Araujo, S.M., 2000. The basement of the brasilia Fold belt and the Goias magmatic Arc. In: Cordani, U.G., Milani, E.J., Thomaz Filho, A., Campos, D.A. (Eds.), Tectonic Evolution of South America. Rio de janeiro. 31st International Geological Congress, Rio de Janeiro, Brazil, pp. 195–229.

Pimentel, M.M., Rodrigues, J.B., Della Giustina, M.E.S., Junges, S.L., Matteini, M., 2011. The tectonic evolution of the Brasilia Belt, central Brazil, based on SHRIMP and LA-ICPMS U–Pb sedimentary provenance data. Journal of South American Earth Sciences. doi:10.1016/j.jsames.2011.02.011.

Piñan-Llamas, A., Simpson, C., 2006. Deformation of Gondwana margin turbidites during the Pampean orogeny, north-central Argentina. Geological Society of America Bulletin 118, 1270–1279.

Quenardelle, S., Ramos, V.A., 1999. The Ordovician Western Sierras Pampeanas Magmatic Belt: record of Argentine Precordillera accretion. Geological Society of London Special Paper 336, 63–86.

Ramos, V.A., 1986. El diastrofismo ocloyico: un ejemplo de tectonica de collision durante el Eopaleozoico en el Noroeste Argentino. Rev. Inst. Cienc. Geolo. 6, 13–28.

Ramos, V.A., 1988. Tectonics of the Late Proterozoic – Early Paleozoic: a collisional history of Southern South America. Episodes 11, 168–174.

Ramos, V.A., Escayola, M., Mutti, D., Vujovich, Y.G., 2000. Proterozoic–Early Paleozoic ophiolites in the Andean basement of southern South America. In: Dilek, Y., Moores, E. (Eds.), Ophiolites and Oceanic Crust: New Insights from Field Studies and Ocean Drilling Program. Geological Society of America Memoir/Special Paper 349. Don Elthon, A Nicolas, pp. 331–349.

Ramos, V.A., 2008. The basement of the central Andes: the Arequipa and related terranes. Annual Review of Earth and Planetary Sciences 36, 289–324.

Ramos, V.A., Vujovich, G., Martino, R., Otamendi, J., 2010. Pampia: a large cratonic block missing in the Rodinia supercontinent. Journal of Geodynamics 50, 243–255.

Rapela, C.W., Pankhurst, R.J., Casquet, C., Baldo, E., Saavedra, J., Galindo, C., 1998. Early evolution of the Proto-Andean margin of South America. Geology 26, 707–710.

Rapela, C.W., Pankurst, R., Casquet, C., Fanning, C., Baldo, E., González Casado, J., Galindo, C., Dahlquist, J., 2007. The Rio de la Plata Craton and the assembly of SW Gondwana. Earth-Science Reviews 83, 49–82.

Roddick, J.C., Loveridge, W.D., Parrish, R.R., 1987. Precise U-Pb dating of zircon at the sub-nanogram Pb level. Chemical Geology 66, 111–121.

Schwartz, J.J., Gromet, L.P., 2004. Provenance of a late Proterozoic-early Cambrian basin, Sierras de Córdoba, Argentina. Precambrian Research 129, 1–21.

Schwartz, J., Gromet, L., Miro, R., 2008. Timing and duration of the Calc-Alkaline Arc of the Pampean Orogeny implications for the Late neoproterozoic to Cambrian evolution of Western Gondwana. The Journal of Geology 116, 39–61.

Segerstrom, K., Turner, J., 1972. A conspicuous flexure in regional structural trend in the Puna of Northwestern Argentine. In: U.S. Geological Survey Professional Paper, 800B 205–209.

Stacey, J.S., Kramers, J.D., 1975. Approximation of terrestrial lead isotope evolution by a two stage model. Earth Planetary Science Letters 26, 207–221.

Stern, R.A., Amelin, Y., 2003. Assesment of errors in SIMS zircon U–Pb geochronology using a natural zircon standard and NIST 610 glass. Chemical Geology 197, 11–142.

Stone, P., Floyd, J.D., Barnes, R.P., Lintern, B.C., 1987. A sequential back-arc and foreland basin thrust duplex model for the southern Uplands of Scotland. Journal of the Geological Society of London 144, 753–764.

Thomas and Astini, 1996.

Tohver, E., van der Pluijm, B.A., van der Voo, R., Rizotto, G., Scandolara, J.E., 2002. Paleogeography of the Amazon craton at 1.2 Ga: early Grenvillian collision with de Llano segment of Laurentia. Earth and Planetary Science Letters 199, 185–200.

Tohver, E., Bettencourt, J.S., Tosdal, R., Mezger, K., Leite, W.B., Payolla, B.L., 2004. Terrane transfer during the Grenvillian orogeny: tracing the Amazon ancestry of southern Appalachian basement through Pb and Nd isotopes. Earth and Planetary Science Letters 228, 161–176.

Turner, J.C., 1960. Estratigrafía de la Sierra de Santa Victoria (Argentina). Boletín de la Academia Nacional de Ciencias en Córdoba 41, 163–196.
Turner, J.C., 1964. Descripcion Geologica de la Hoja 2c santa Victoria (Provincias de salta y Jujuy). Carta geologico-economica de la republica Argentina Escala 1:200.000, 100 pp.
Van Staal, C.R., Dewey, J.F., MacNiocaill, C., McKerrow, S., 1998. The Cambrian–Silurian tectonic evolution of the northern Appalachians: history of a complex, southwest Pacific-type segment of Iapetus. In: Blundell, D.J., Scott, A.C. (Eds.), In Lyell: The Past is The Key to the Present. Geological Society Special Publication 143, pp. 199–242.
Van Staal, C.R., Rogers, N., Taylor, B.E., 2001. Formation of low temperature mylonites and phyllonites by alkali-metasomatic weakening of felsic volcanic rocks during a progressive, subduction-related deformation. Journal of Structural Geology 23, 903–921.
Van Staal, C.R., Whalen, J.B., Valverde-Vaquero, P., Zagorevski, A., Rogers, N., 2009. Pre-Carboniferous, episodic accretion-related, orogenesis along the Laurentian margin of the northern Appalachians. In: Murphy, J.B., Keppie, J.D., Hynes, A.J. (Eds.), Ancient Orogens and Modern Analogues. Geological Society London Special Publication 327, pp. 271–316.
Van Staal, C.R., Currie, K.L., Rowbotham, G., Goodfellow, W., Rogers, N., 2008. P-T paths and exhumation of Late Ordovician-Early Silurian blueschists and associated metamorphic nappes of the Salinic Brunswick subduction complex, northern Appalachians. Geological Society of America Bulletin 120, 1455–1477.
Viramonte, J., Becchio, J., Coira, B., Aramayo, C., 1993. Aspectos pretrologicos y geoquimicos del Basamento Preordovicico del Borde Oriental de la Puna Austral. XII Congreso geologico Argentino. Actas 4, 307–318.
Waldron, J.W.F., van Staal, C.R., 2001. Taconic Orogeny and the accretion of the Dashwoods block: a peri-Laurentian microcontinent in the Iapetus Ocean. Geology 29, 811–814.
Willner, A.P., Lottner, U.S., Miller, H., 1987. Early Paleozoic structural development in the NW Argentine basement of the Andes and its implications for geodynamic reconstructions. in Gondwana six: structure, tectonics, and geophysics. Geophysical Monograph 40, 229–239.
Winchester, J.A., Floyd, P.A., 1977. Geochemical discrimination of different magma series and their differentiation products using immobile elements. Chemical Geology 20, 325–343.
Wood, D.A., 1980. The application of a Th-Hf-Ta diagram to problems of tectonomagmatic classification and to establishing the nature of crustal contamination of basaltic lavas of the British Tertiary volcanic province. Earth and Planetary Science Letters 50, 11–30.
Wood, D.A., Tarney, J., Saunders, A.D., Bougault, H., Joron, J.L., Treuilet, M., Cann, J.R., 1979. Geochemistry of basalts drilled in the north Atlantic by IPOD Leg. 49: implications for mantle heterogeneity. Earth and Planetary Science Letters 42, 77–79.
Zimmermann, U., 2005. Provenance studies of very low-to low-grade metasedimentary rocks of the Puncoviscana Complex, northwest Argentina. In: Vaughan, A., Leat, P., Pankhurst, R. (Eds.), Geological Society of London. Special Publication 246, pp. 381–416.